The IRM
Quarterly
Winter 2017-18, Vol. 27 No.4

ISSN: 2152-1972

Inside...

Magnetic tests and characterization protocols: mineralogy and grain size / domain state Part I: isothermal strong field tests

Mike Volk, Mike Jackson and Dario Bilardello

Institute for Rock Magnetism
mvolk@umn.edu

Rocks are solid mineral assemblages formed under varying conditions at different times of Earth's history. They help us understand the processes that shaped our planet and other extraterrestrial bodies. Few minerals are magnetic, the most important being magnetite. Locked in a matrix of "non-magnetic" material, these (typically) ferri-magnetic minerals, when larger than a mineral-specific threshold-size, carry a remanent magnetization. Their remanence tells the story of how the magnetic field direction and/or intensity has changed with time. Much of paleo- and planetary-magnetism relies on the unaltered remanence state of a rock or meteorite to draw conclusions about the origin of that magnetization. However, even if a rock contains magnetic minerals and carries a magnetization, it is not given that the remanence reflects a primary magnetization, and is consequently trustworthy.

Rock magnetism tries to understand how these particle systems are able to retain magnetic information over millions, sometimes billions of years and what processes can alter their state. Decades of work has been put into understanding why some rocks are better at recording magnetic fields than others. One of the most important factors is the size, or to be more precise the magnetic domain state, of the magnetic particles contained in a rock. Paleomagnetists are not the only scientists interested in the size of magnetic particles. From the material sciences to environmental magnetism, grain-size dependent magnetic properties play an important role. Magnetic grain-size may be used as a proxy for climatic changes and can be used to reconstruct the environment at the time of their genesis or deposition. Environmental magnetism, for example, uses the quasi continuous record of sediments to explore relative changes of the sediment sources and/or depositional and post-depositional conditions through time. Often the question of where the sediments' magnetic particles come from may be answered by investigating their rock magnetic properties. The same principle has also been used by archeomagnetists to trace the provenance of artifacts constructed with geological materials. With such a wide variety of sample materials, such as rocks and meteorites, fresh lake or marine sediments, loess, soils, and even magnetotactic bacteria, the particle sizes in question can be equally broad.

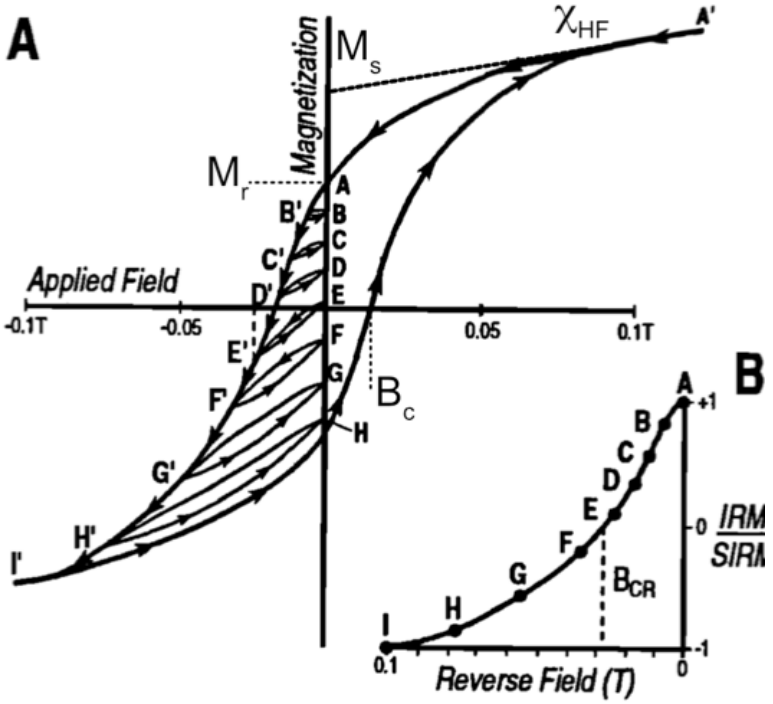

Figure 1: Hysteresis processes and quantities. On removal of a positive saturating field the magnetization decreases from ferromagnetic saturation (A') to M_r (A). Continued sweeping of the field toward large negative values drives the magnetization toward $-M_s$. Interrupting the sweep and turning the field off at reversal fields (B' to I') produces the set of backfield remanences (B to I) and minor loops B-B', C-C', etc. The field-axis intercept of the loop (i.e., point at which the magnetization is reduced to zero, between D' and E') is the coercive force (B_c). The reverse field which reduces the remanence to zero (i.e., between E and F) is the coercivity of remanence (B_{cr}). Modified after Roberts (1995) and Thompson and Oldfield (1986).

Domain state boundaries are mineral dependent. Extremely small particles, usually in the low nm range, are in a so-called superparamagnetic (SP) state. They behave similarly to a paramagnetic grain as they can not record magnetic fields, but they share the same saturation magnetization as their larger counterparts. The inability to

cont'd. on pg. 13...

Visiting Fellow Reports

Characterisation of palaeomagnetic remanence carriers in palaeokarst sediments from southern Africa

Tom Mallett

The Australian Archaeomagnetism Laboratory, Department of Archaeology and History, La Trobe University, Melbourne, Australia

tlmallett@students.latrobe.edu.au

Plio-Pleistocene cave infill deposits of dolomitic karst systems in southern Africa have been the target of magnetobiostratigraphic age assessments since the late 1970s (e.g. Brock et al. 1977). In more recent years, palaeomagnetic analyses have been undertaken in conjunction with uranium-lead and uranium-thorium dating, electron spin resonance, cosmogenic nuclide burial dating and biochronology to obtain more refined multiproxy age estimates for the cave fills (see chronological reviews in Herries et al. 2009; 2013). These UNESCO World Heritage listed sites, which are for the most part located just northwest of Johannesburg, are known for their abundant preservation of early hominin (Australopithecus, Paranthropus and Homo) and other extinct fossil taxa, along with some of the earliest archaeological traces found in South Africa (Early Stone Age lithic technology and bone tools).

Palaeomagnetic analysis at these sites has long been complicated by a number of factors. Many of the caves occur in relict, collapsed states (palaeokarst), affected by widespread landscape erosion, along with mining activities during the early 20th century. Some sites have also undergone multiple phases of karstification through more ancient portions of the cave fills that obscure already complex stratigraphic relationships that can exist in caves (e.g. Sterkfontein; Herries & Shaw 2011). Further, brecciated deposits that often dominate the stratigraphy (e.g. talus sediments) have been shown to exhibit randomised remanence directions due to their deposition by collapse (Herries et al. 2006). This leaves fine-grained (calcified) fluvial sediment and speleothem components that can be suitably targeted for palaeomagnetism. Whilst these deposits often record stable depositional and post-depositional magnetisations, they usually exist in short and disconnected stratigraphic sequences that vary laterally across the sites, opening the potential for gaps in the magnetostratigraphy. An additional complicating factor is that samples often exhibit substantial low coercivity viscous overprinting within ultrafine superparmagnetic (SP) grains that occur in high concentrations within the cave sediments (considered a product of long term burning and weathering of the South African landscape; Herries et al. 2006). This has been particularly problematic for obtaining secure age estimates at sites such as the Australopithecus africanus bearing Makapansgat Limeworks (Herries et al. 2013). In addition, we at present have only a limited understanding on the effects of karst-specific diagenetic processes (e.g. secondary calcite induration, calcification and recrystallisation) on the acquisition, alteration and lock-in times for cave sediment magnetisations.

Despite these problems, some significant palaeomagnetic records have been obtained from palaeokarst sites that have been central to constructing robust chronostratigraphies. Short geomagnetic excursions and high resolution transitional field states have been recorded in rapid depositional rate sequences that correlate well to polarity timescales with chronometric ages (Pickering et al. 2011 and manuscript in preparation). Flowstones in particular, which can be directly dated via uranium-series and suffer less in the way of post-depositional alterations (Lascu & Feinberg 2011), often record short duration events, especially between ~2.2 and 1.95 Ma when many sites were undergoing active sedimentation during periods of increased geomagnetic instability (Herries & Shaw 2011; Singer 2014). To date, evidence for the Huckleberry Ridge event has been documented at two sites (Dirks et al. 2010; Herries and Shaw 2011) as well as potentially the Réunion and pre-Olduvai events (Herries and Shaw 2011; Pickering et al. 2011). The identification of polarity reversals also allows for a reduction in large absolute age error margins for stratigraphic units when reversal boundaries are located within close stratigraphic proximity to dated samples (Herries et al. 2018). As part of continuing chronological work at these localities, we sought to undertake more detailed rock magnetic experiments to determine what mineral phases were holding the palaeomagnetic signal, and whether these had been subject to diagenetic alteration that could affect correct magnetostratigraphic correlation. This was stimulated in particular by recent work on older deposits that show more complex overprinting and lower unblocking temperature magnetisations than previously identified at younger sites (e.g. Herries et al. 2018). We bought samples to the Institute for Rock Magnetism (IRM) from a number of different South African cave systems (Drimolen, Bolt's Farm, Malapa, Coopers, Makapansgat, Haasgat and Hoogland; ~5–4 to 1.6–1.4 Ma age range) as a 'regional palaeokarst sample', to assess inter-site variation in iron oxide minerology, concentration, domain state and grain size. These have also served as a control sample set to integrate additional characterisation methods (e.g. Raman micro-spectroscopy, electron microscopy). We have also more extensively sampled deposits at Makapansgat Limeworks and Haasgat to help clarify their magnetostratigraphic profiles. At the IRM, we measured hysteresis loops and backfield curves, first order reversal curves (FORCs), high temperature magnetic susceptibility (χT) on the Kappabridge (in air to 700°C), and various low temperature remanence and susceptibility sweeps on the MPMS XL and 5S units. These are being linked with measurements undertaken

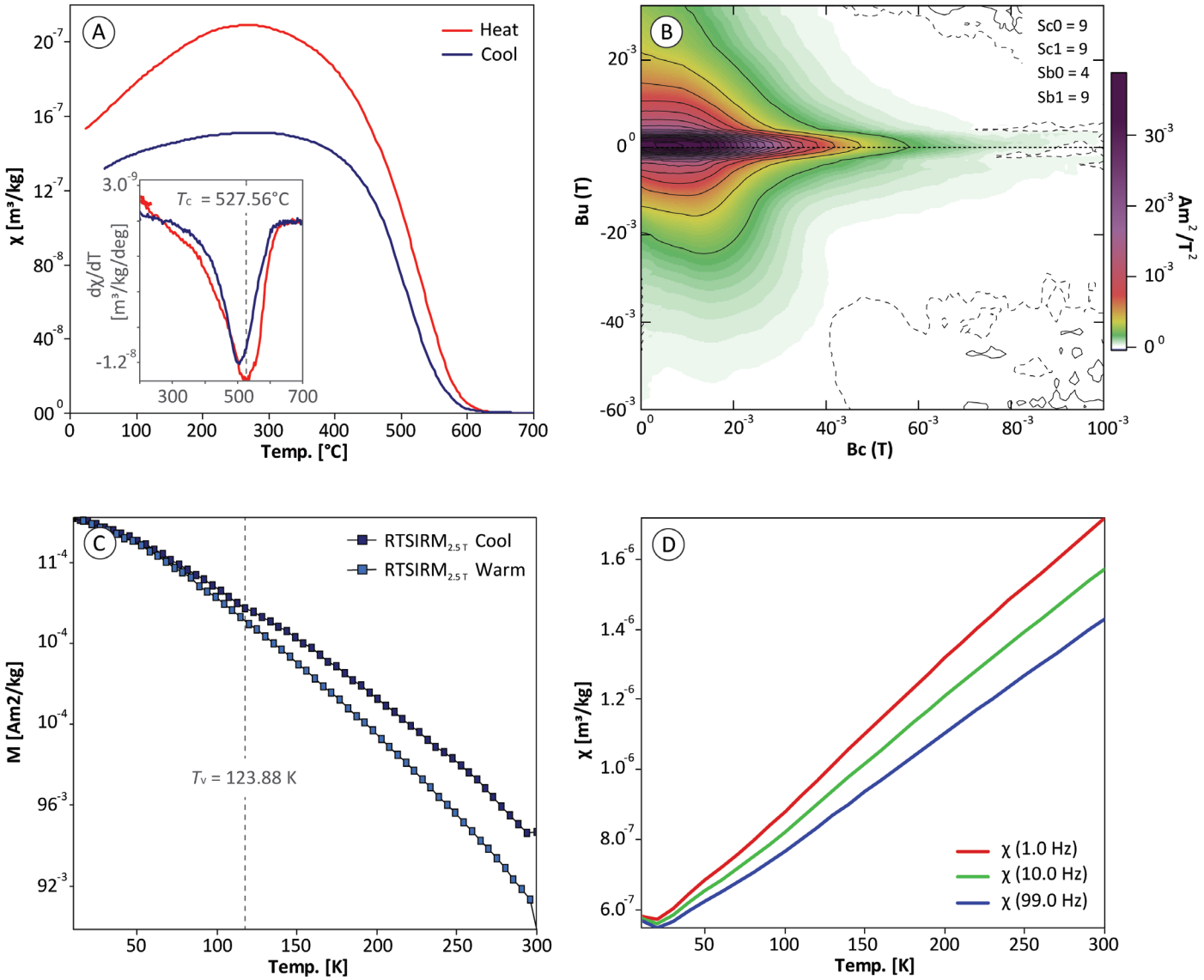

Figure 1: Rock magnetic data for palaeokarst at the Drimolen Makondo (adapted from Herries et al. 2018). A) High temperature magnetic susceptibility with a derivative plot insert and Tc estimate. B) FORC diagram. C) RT SIRM low temperature data. D) Low temperature magnetic susceptibility measurements at varying frequencies.

at The Australian Archaeomagnetism Laboratory (www.archaeomagnetism.com), including alternating field demagnetisation (AFD), thermal demagnetisation (THD), and combined AFD/THD strategies, 3-axis isothermal remanent magnetisation THD, and viscous remagnetisation tests.

Results show that the regional palaeokarst samples have a consistent minerology across the different localities; Figure 1 shows a representative example from the ~2.6 Ma Drimolen Makondo (Herries et al. 2018). FORC diagrams (Figure 1B) highlight that the samples are dominated by a low coercivity remanence in a single domain (SD) to vortex state (Roberts et al. 2017) grain size range. SD contributions are shown from closed concentric contours along the central ridge of the FORC, while vortex state magnetisations are inferred from remanence intensities with a broader spread away from the central ridge along the Bu axis and weak lobe-like features. There is minimal evidence for remanence contributions from multi-domain (MD) particles, which would display a vertical spread along the B_u FORC axis. χT and low temperature remanence experiments indicate that these low coercivity magnetisations are carried by impure forms of magnetite or maghemite. Curie temperatures (T_c), estimated from the 1st derivative minima of χT heating curves, range from 380–550°C (mean of 490°C). The bulk of samples also show subtle inflections close to the Verway transition (T_v) in magnetite (~120 K; Figure 1C), suggestive of Ti-substitution in the crystal lattice or potentially oxidisation (maghemisation) effects. Increased Ti-substitution in magnetite also functions to lower the T_c which likely explains the χT estimates. Low temperature measurements also indicate the presence of goethite in almost all samples as highlighted by increases in magnetisation at lower temperatures, the spread between 2.5 TFC-ZFC remanence curves, and largely reversible RT SIRM curves. Whilst high coercivity remanences are typically seen in these sites via the non-saturation of isothermal remanent magnetisation curves, this is the first time goethite has been identified magnetically at these sites. The high coercivity components have typically been interpreted as relating to pig-

mentary hematite given the red colouration of the sediments (e.g. Herries et al. 2006), which does not usually contribute to the natural remanent magnetisation (NRM) of the samples. There was no substantive evidence for a Morin transition in hematite (260–250 K), which similar to the T_v, can also be supressed by substitution as well as when it occurs in ultrafine grain sizes such as pigmentary forms. Additionally, low temperature magnetic susceptibility (χ) sweeps on warming from 20–300 K show a strong frequency dependence on χ, likely relating to ultrafine SP grains that dominate South African palaeokarst sediments (Figure 1D).

We are currently testing for any goethite influence on the NRM, which would likely be a secondary chemically formed remanence, via thermal pre-treatments to ~160°C of AFD samples and comparison to conventional AFD on sister specimens. As for lower unblocking temperature magnetisations, these likely relate to increased Ti content in magnetite (or variable T_c maghemite), perhaps related to influence of local intrusive volcanics on ancient sediment sources (Herries et al. 2018). It is clear however from THD spectra that multiple unblocking temperature components reflective of detrital minerals can exist within the same sample, often recording the same directions, implying that their magnetisations were locked-in coevally.

Acknowledgements

Thanks to everyone at the IRM for being so kind and welcoming, and for offering the Visiting Research Fellowship – especially Dario Bilardello, Mike Jackson and Joshua Feinberg for showing me the ropes with the instruments/software and for the helpful chats along the way. I also acknowledge the Australian Postgraduate Award and La Trobe University Internal Research Grant for helping to pay my way while in the US. The collection of samples was obtained under Australian Research Council Future Fellowship FT120100399.

References

Brock, A., P. L. McFadden and T. C. Partridge 1977 Preliminary palaeomagnetic results from Makapansgat and Swartkrans. Nature 266:249–250.

Dirks, P. H. G. M., J. M. Kibii, B. F. Kuhn, C. Steininger, S. E. Churchill, J. D. Kramers, R. Pickering, D. L. Farber, A. Mériaux, A. I. R. Herries, G. C. P. King and L. R. Berger 2010 Geological setting and age of Australopithecus sediba from southern Africa. Science 328:205–208.

Herries, A. I. R. and J. Shaw 2011 Palaeomagnetic analysis of the Sterkfontein palaeocave deposits: implications for the age of the hominin fossils and stone tool industries. Journal of Human Evolution 60:523–539.

Herries, A. I. R., K. E. Reed, K. L. Kuykendall and A. G. Latham 2006 Speleology and magnetobiostratigraphic chronology of the Buffalo Cave fossil site, Makapansgat, South Africa. Quaternary Research 66:233–245.

Herries, A. I. R., D. Curnoe and J. W. Adams 2009 A multi-disciplinary seriation of early Homo and Paranthropus bearing palaeocaves in southern Africa. Quaternary International 202:14–28.

Herries, A. I. R., R. Pickering, J. W. Adams, D. Curnoe, G. Warr and A. G. Latham 2013 A multi-disciplinary perspective on the age of Australopithecus in southern Africa. In K. E. Reed, J. G. Fleagle and R. E. Leakey (eds):21–40. The Paleobiology of Australopithecus, New York: Springer.

Herries, A. I. R., A. Murszewski, R. Pickering, T. Mallett, R. Joannes-Boyau, B. Armstrong, J. W. Adams, S. Baker, A. Blackwood, P. Penzo-Kajewski, P. Hopley, P. Kappen, A. B. Leece, J. Martin, D. Rovinski and G. Boschian 2018 Geoarchaeological and 3D Visualisation approaches for contextualising in-situ fossil bearing palaeokarst in South Africa: a case study from the ~2.61 Drimolen Makondo. Quaternary International. In Press.In Press.

Lascu, I. and J. M. Feinberg 2011 Speleothem magnetism. Quaternary Science Reviews 30:3306–3320.

Pickering, R., P. H. G. M. Dirks, Z. Jinnah, D. J. de Ruiter, S. E. Churchill, A. I. R. Herries, J. D. Woodhead, J. C. Hellstrom and L. R. Berger 2011 Australopithecus sediba at 1.977 Ma and implications for the origin of the genus Homo. Science 333:1421–1423.

Roberts, A. P., T. P. Almeida, N. S. Church, R. J. Harrison, D. Heslop, Y. Li, J. Li, A. R. Muxworthy, W. Williams and X. Zhao 2017 Resolving the origin of pseudo-single domain magnetic behavior. Journal of Geophysical Research: Solid Earth doi: 10.1002/2017JB014860

Singer, B. S. 2014 A Quaternary geomagnetic instability timescale. Quaternary Geochronology 21:29–52.

Diagenetic degradation of paleoenvironmental signals in magnetic susceptibility in the northern Bay of Bengal

Steve Phillips

Institute for Geophysics, Jackson School of Geosciences, University of Texas at Austin, Austin, TX, USA

phillips.stephen.c@gmail.com

We measured rock magnetic properties on sediment core samples from two sites in the offshore Mahanadi Basin, India, drilled in 2015 during International Ocean Discovery Program (IODP) Expedition 353 (Clemens et al., 2016). These sites, U1445 and U1446, are 96 and 75 km offshore and in 2502 and 1430 m water depth respectively. Shipboard magnetic susceptibility (κ) from whole round core logging shows down core cyclic variability that may potentially represent a monsoon-driven paleoenvironmental signal. However, below the sulfate-methane transition zone (SMTZ) at ~20 m below sea floor (msbf) at both sites, κ decreases and the signal becomes diminished (Fig. 1). This effect is most pronounced at Site U1445. Is this change driven by an increase in the transport and deposition of ferrimagnetic minerals with time? Or is it driven by an onset of alteration at depth? We hypothesize that the primary detrital magnetic mineral assemblage has been altered by hydrogen sulfide produced by organoclastic sulfate reduction and/or anaerobic oxidation of methane, as has been observed in other methane-bearing continental margin sediments (e.g. Housen and Musgrave, 1996; Riedinger

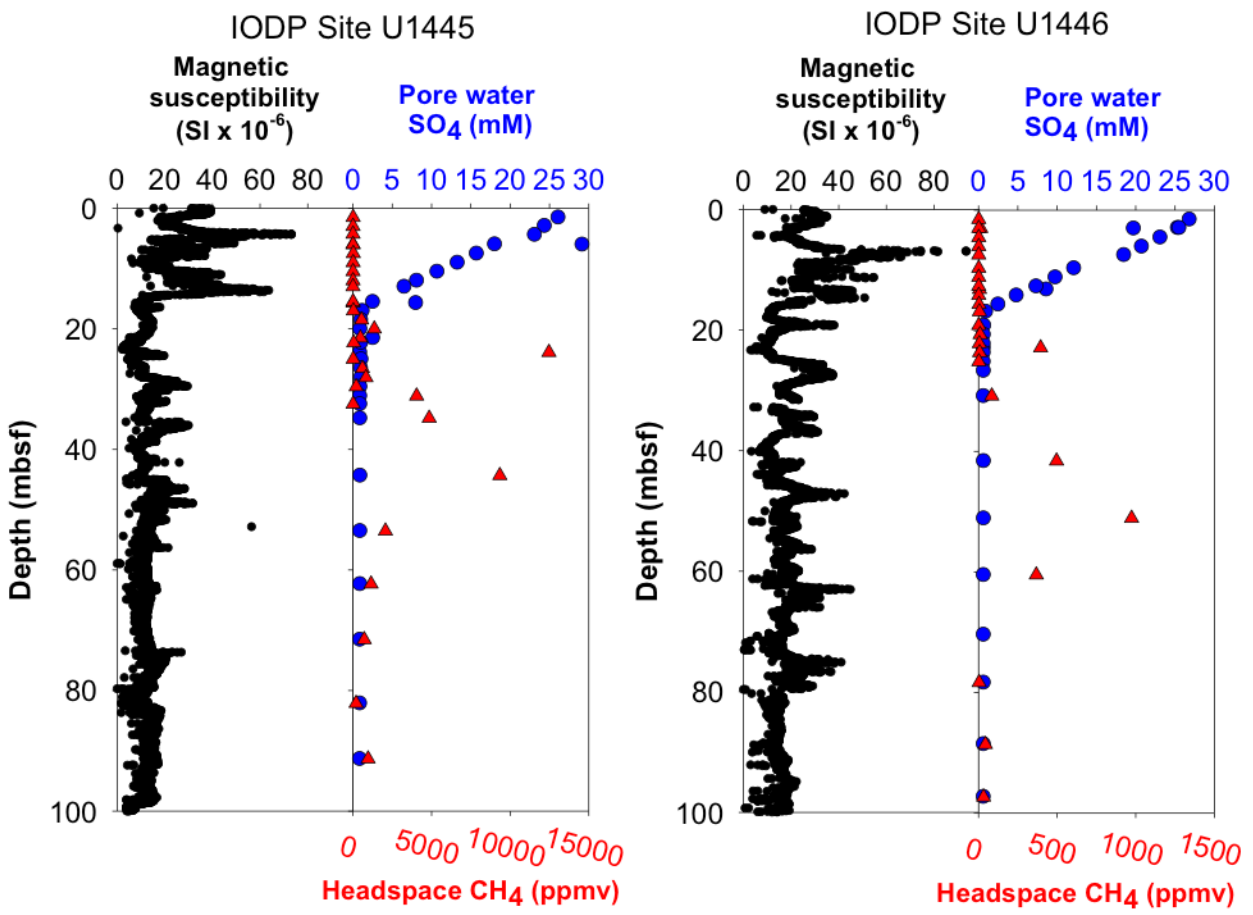

Figure 1. Down core variation in magnetic susceptibility, pore water sulfate, and headspace methane at IODP Sites U1445 and U1446 in the northern Bay of Bengal (Clemens et al., 2016). The sulfate-methane transition zone (SMTZ) is near ~20 m below seafloor (msbf) at both sites. Note the lower amplitude in the cyclic variation at Site U1445.

et al., 2005).

In order to test this hypothesis and determine the extent to which the magnetic signal has been altered, we measured multiple magnetic properties at the IRM that will be integrated with ongoing sulfur and carbon geochemistry measurements. At the IRM, we measured magnetic susceptibility (room temperature and high temperature sweeps with the KappaBridge), hysteresis loops with a vibrating sample magnetometer (VSM), anhysteretic remanent magnetism (ARM), and low temperature remanence curves with the magnetic properties measurement system (MPMS).

The magnetic susceptibility measured in the lab confirmed the pattern measured at sea. MPMS measurements suggest a primary magnetic mineral assemblage composed of magnetite and goethite, based on the deviation between the field-cooled (FC) and zero field-cooled (ZFC) remanences and the presence of the Verwey transition (Fig. 2). Variation in the low-temperature remanence curves between samples shows the relative variation in these minerals down core. Hysteresis parameters suggest the presence of pseudo-single domain magnetite. All samples measured with high temperature sweeps in the KappaBridge showed substantial alteration during heating steps (Fig. 3), even under argon atmosphere, which could be explained by iron sulfides or iron-rich carbonates converting to magnetite during heating. The magnitude of this alteration in magnetic susceptibility during heating was generally higher in deeper samples. ARM results suggest a loss of fine-grained magnetite with depth. We are now continuing to interpret down core patterns and cross-correlations in all magnetic properties to understand potential alteration pathways. The rock magnetic data obtained at the IRM are also being integrated with bulk elemental chemistry and pore water chemistry data to understand the history of magnetic mineral alteration at these sites.

Magnetic susceptibility can be a useful proxy of detrital processes influenced by the Indian monsoon (e.g. Colin et al., 1998; Phillips et al., 2014); however, the potential for mixed detrital and diagenetic influences on these magnetic records must be taken into account, especially in sediment cores that extend to the SMTZ. Our rock magnetic measurements made at the IRM can help determine which intervals of the recovered cores record paleoenvironmental signals and which have been overprinted by diagenetic processes.

Acknowledgements

I would like to thank the University of Minnesota IRM for the support of a Visiting Fellowship, as well as the assistance of Mike Jackson, Dario Bilardello, and Dan Maxbauer. I would also like the thank the support of the UT Institute for Geophysics for additional travel

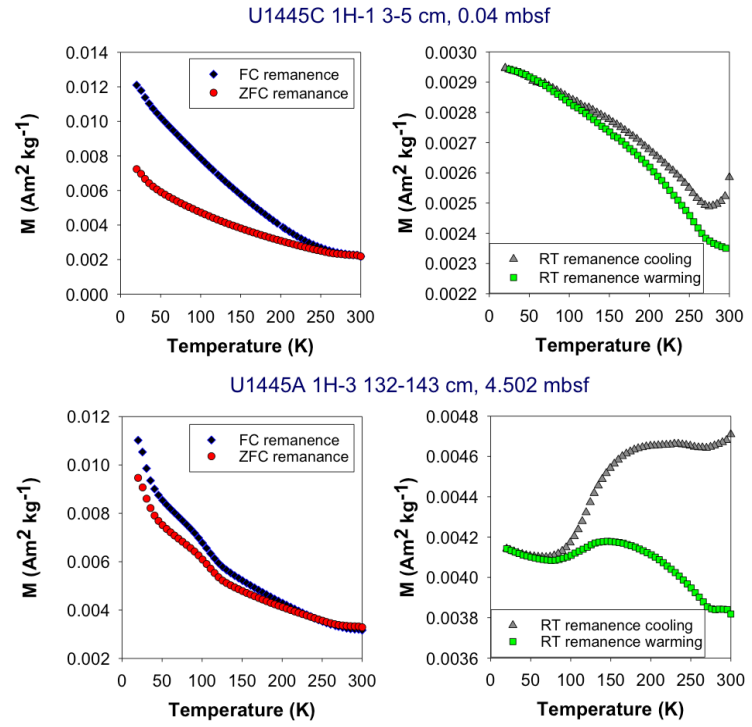

Figure 2. Low-temperature remanence curves from MPMS: field-cooled (FC) remanence, zero field-cooled (ZFC), and room temperature (RT) remanence. These results indicate the presence of goethite and magnetite in the detrital magnetic mineral assemblage.

support, and the support of the Consortium of Ocean Leadership for support through a Post-Expedition Activity Award.

References

Clemens, S.C., Kuhnt, W., LeVay, L.J., and the Expedition 353 Scientists, 2016. Indian Monsoon Rainfall. Proceedings of the International Ocean Discovery Program, 353: College Station, TX (International Ocean Discovery Program). http://dx.doi.org/10.14379/iodp.proc.353.2016

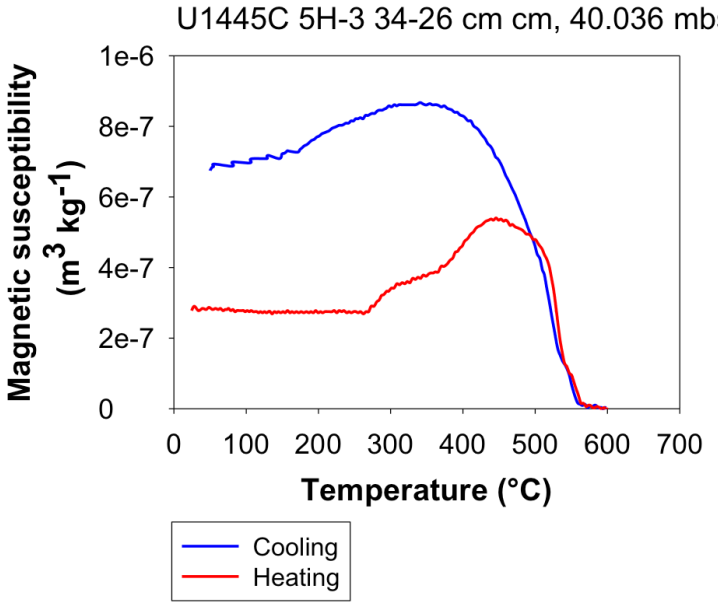

Figure 3. Example of the observed changes in magnetic susceptibility during heating under argon, with an increase at around 300 °C.

Colin, C., Kissel, C., Blamart, D., and Turpin, L., 1998. Magnetic properties of sediments in the Bay of Bengal and the Andaman Sea: impact of rapid North Atlantic Ocean climate events on the strength of the Indian monsoon. Earth and Planetary Science Letters 160, 623-635, https://doi.org/10.1016/S0012-821X(98)00116-2

Housen, B.A., and Musgrave, R. J., 1996. Rock-magnetic signature of gas hydrates in accretionary prism sediments, Earth and Planetary Science Letters, 139, 509-519, https://doi.org/10.1016/0012-821X(95)00245-8

Phillips, S.C., Johnson, J.E., Giosan, L., and Rose, K., 2014. Monsoon-influenced variation in productivity and lithogenic sediment flux since 110 ka in the offshore Mahanadi Basin, northern Bay of Bengal. Marine and Petroleum Geology 58A, 502-525, doi:10.1016/j.marpetgeo.2014.05.007.

Riedinger, N., Pfeifer, K., Kasten, S., Garming, J.F.L., Vogt, C., and Hensen, C., 2005. Diagenetic alteration of magnetic signals by anaerobic oxidation of methane related to a change in sedimentation rate. Geochimica et Cosmochimica Acta. 69, 4117-4126, https://doi.org/10.1016/j.gca.2005.02.004

Current Articles

A list of current research articles dealing with various topics in the physics and chemistry of magnetism is a regular feature of the IRM Quarterly. Articles published in familiar geology and geophysics journals are included; special emphasis is given to current articles from physics, chemistry, and materials-science journals. Most are taken from ISI Web of Knowledge, after which they are subjected to Procrustean culling for this newsletter. An extensive reference list of articles (primarily about rock magnetism, the physics and chemistry of magnetism, and some paleomagnetism) is continually updated at the IRM. This list, with more than 10,000 references, is available free of charge. Your contributions both to the list and to the Current Articles section of the IRM Quarterly are always welcome.

Archeomagnetism

Butler, D. H., and P. C. Dawson (2018), Untangling natural and anthropogenic multi-element signatures in archaeological soils at the Ikirahak site, Arctic Canada, Boreas, 47(1), 189-201.

Holakooei, P., J. F. de Laperouse, M. Rugiadi, and F. Caro (2018), Early Islamic pigments at Nishapur, north-eastern Iran: studies on the painted fragments preserved at The Metropolitan Museum of Art, Archaeological and Anthropological Sciences, 10(1), 175-195.

Oikonomou, A., J. Henderson, M. Gnade, S. Chenery, and N. Zacharias (2018), An archaeometric study of Hellenistic glass vessels: evidence for multiple sources, Archaeological and Anthropological Sciences, 10(1), 97-110.

Biomagnetism

Chen, D. D., T. X. Liu, X. M. Li, F. B. Li, X. B. Luo, Y. D. Wu, and Y. Wang (2018), Biological and chemical processes of microbially mediated nitrate-reducing Fe(II) oxidation by Pseudogulbenkiania sp strain 2002, Chemical Geology, 476, 59-69.

Liu, G. F., H. L. Yu, N. Wang, R. F. Jin, J. Wang, and J. T. Zhou (2018), Microbial reduction of Ferrihydrite in the presence of reduced Graphene oxide materials: Alteration of Fe(III) reduction rate, biomineralization product and settling behavior, Chemical Geology, 476, 272-279.

Malherbe, C., I. B. Hutchinson, R. Ingley, A. Boom, A. S. Carr, H. Edwards, B. Vertruyen, B. Gilbert, and G. Eppe (2017), On the Habitability of Desert Varnish: A Combined Study by Micro-Raman Spectroscopy, X-ray Diffraction, and Methylated Pyrolysis-Gas Chromatography-Mass Spectrometry, Astrobiology, 17(11), 1123-1137.

Usui, Y., T. Yamazaki, and M. Saitoh (2017), Changing Abundance of Magnetofossil Morphologies in Pelagic Red Clay Around Minamitorishima, Western North Pacific, Geochemistry Geophysics Geosystems, 18(12), 4558-4572.

Environmental magnetism and Climate

Abbasi, S., B. Keshavarzi, F. Moore, H. Delshab, N. Soltani, and A. Sorooshian (2017), Investigation of microrubbers, microplastics and heavy metals in street dust: a study in Bushehr city, Iran, Environmental Earth Sciences, 76(23).

Achilles, C. N., et al. (2017), Mineralogy of an active eolian sediment from the Namib dune, Gale crater, Mars, Journal of Geophysical Research-Planets, 122(11), 2344-2361.

Adnani, M., M. A. Azzaoui, H. Elbelrhiti, M. Ahmaniou, and L. Masmoudi (2018), Investigation of reddening patterns of dune sands - The megabarchans of Al-ghord Lahmar (Khnifiss National Park, South-West of Morocco), Catena, 162, 230-244.

Attia, A. H., S. A. El-Sayed, and M. E. El-Sabagh (2018), Utilization of GIS modeling in geoenvironmental studies of Qaroun Lake, El Fayoum Depression, Egypt, Journal of African Earth Sciences, 138, 58-74.

Bakhmutov, V. G., A. Y. Kazanskii, G. G. Matasova, and D. V. Glavatskii (2017), Rock magnetism and magnetostratigraphy of the loess-sol series of Ukraine (Roksolany, Boyanychi, and Korshev sections), Izvestiya-Physics of the Solid Earth, 53(6), 864-884.

Bautista, F., M. F. Bogalo, A. S. Navarro, A. Goguitchaichvili, M. J. D. Iniesta, R. Cejudo, P. M. Sanleandro, J. M. Gil, and E. Diaz-Pereira (2018), Magnetic and pedological characterisation of a paleosol under aridic conditions in Spain, Studia Geophysica Et Geodaetica, 62(1), 139-166.

Clift, P. (2017), Cenozoic sedimentary records of climate-tectonic coupling in the Western Himalaya, Progress in Earth and Planetary Science, 4.

Cui, M., Z. H. Wang, K. N. Rao, S. J. Sangode, Y. Saito, T. Chen, Y. R. Kulkarni, K. Kumar, and G. Demudu (2017), A mid- to late-Holocene record of vegetation decline and erosion triggered by monsoon weakening and human adaptations in the south-east Indian Peninsula, Holocene, 27(12), 1976-1987.

Eker, C. S. (2017), Geochemical and isotopic characteristics of stream and terrace sediments of the Harsit Stream, NE Turkey, Geochemistry-Exploration Environment Analysis, 17(4), 279-296.

Frei, R., L. N. Dossing, C. Gaucher, P. C. Boggiani, K. M. Frei, T. B. Arting, S. A. Crowe, and B. T. Freitas (2017), Extensive oxidative weathering in the aftermath of a late Neoproterozoic glaciation - Evidence from trace element and chromium isotope records in the Urucum district (Jacadigo Group) and Puga iron formations (Mato Grosso do Sul, Brazil), Gondwana Research, 49, 1-20.

Gao, X. B., et al. (2018), The different climatic response of pedogenic hematite and ferrimagnetic minerals: Evidence from particle-sized modern soils over the Chinese Loess Plateau, Quaternary Science Reviews, 179, 69-86.

Ge, C., W. G. Zhang, C. Y. Dong, F. Wang, H. Feng, J. G. Qu, and L. Z. Yu (2017), Tracing Sediment Erosion in the Yangtze River Subaqueous Delta Using Magnetic Methods, Journal of Geophysical Research-Earth Surface, 122(11), 2064-2078.

Guo, Y. C., Y. Song, X. X. Fang, X. Q. Pang, and T. T. Li (2018), Reservoir characterization of an organic-rich dolomitic tight-oil reservoir, the Lower Cretaceous Xiagou Formation in the Qingxi Sag, Jiuquan Basin, NW China, Marine and Petroleum Geology, 89, 541-559.

Hosek, J., L. Lisa, U. Hambach, L. Petr, L. Vejrostova, A. Bajer, T. M. Grygar, P. Moska, Z. Gottvald, and M. Horsak (2017), Middle Pleniglacial pedogenesis on the northwestern edge of the Carpathian basin: A multidisciplinary investigation of the Bina pedo-sedimentary section, SW Slovakia, Palaeogeography Palaeoclimatology Palaeoecology, 487, 321-339.

Hunt, A., F. Oldfield, J. Bloemendal, J. F. Boyle, R. C. Chiverrell, R. Lyons, Z. Shen, E. R. Williams, and W. Balsam (2017), To what extent have laterites contributed to the geochemical, surface reflectance and magnetic properties of adjacent tropical soils? Evidence from Niger and Burkina Faso, Earth Surface Processes and Landforms, 42(15), 2554-2569.

Jordanova, N. (2017), magnetism of materials occurring in the environment-basic overview, 1-28 pp.

Jordanova, N. (2017), magnetism of soils from the antarctic

peninsula, 331-347 pp.
Jordanova, N. (2017), magnetism of soils with clay-enriched subsoil: luvisols, alisols, and acrisols, 65-138 pp.
Jordanova, N. (2017), the magnetism of soils with little or no profile differentiation: soils from mountain areas (cambisols, umbrisols) and floodplains (fluvisols), 287-330 pp.
Jordanova, N. (2017), the discriminating power of soil magnetism for the characterization of different soil types, 349-365 pp.
Khan, R., M. A. Rouf, S. Das, U. Tamim, K. Naher, J. Podder, and S. M. Hossain (2017), Spatial and multi-layered assessment of heavy metals in the sand of Cox's-Bazar beach of Bangladesh, Regional Studies in Marine Science, 16, 171-180.
Kong, L. W., H. M. Sayem, and H. H. Tian (2018), Influence of drying-wetting cycles on soil-water characteristic curve of undisturbed granite residual soils and microstructure mechanism by nuclear magnetic resonance (NMR) spin-spin relaxation time (T-2) relaxometry, Canadian Geotechnical Journal, 55(2), 208-216.
Krainov, M. A., E. V. Bezrukova, E. V. Kerber, O. V. Levina, E. V. Ivanov, A. A. Shchetnikov, and I. A. Filinov (2017), First results of study of Lake Baunt bottom sediments (northern Transbaikalia), Russian Geology and Geophysics, 58(11), 1401-1411.
Lacasse, C. M., R. V. Santos, E. L. Dantas, Q. Vigneron, I. M. C. de Sousa, V. Harlamov, M. A. Lisniowski, I. B. M. Pessanha, E. P. Frazao, and J. A. D. Cavalcanti (2017), Sr-87/Sr-86 dating and preliminary interpretation of magnetic susceptibility logs of giant piston cores from the Rio Grande Rise in the South Atlantic, Journal of South American Earth Sciences, 80, 244-254.
Land, J. S., H. Tsikos, D. Cousins, G. Luvizotto, and T. Zack (2018), Origin of red beds and paleosols in the Palaeoproterozoic Transvaal and Olifansthoek Supergroups of South Africa: provenance versus metasomatic controls, Geological Journal, 53(1), 191-202.
Li, Y., H. B. Zhang, C. Tu, and Y. M. Luo (2018), Magnetic characterization of distinct soil layers and its implications for environmental changes in the coastal soils from the Yellow River Delta, Catena, 162, 245-254.
Liu, X. T., A. C. Li, J. Dong, J. Lu, J. Huang, and S. M. Wan (2018), Provenance discrimination of sediments in the Zhejiang-Fujian mud belt, East China Sea: Implications for the development of the mud depocenter, Journal of Asian Earth Sciences, 151, 1-15.
Lukens, W. E., S. G. Driese, D. J. Peppe, and M. Loudermilk (2017), Sedimentology, stratigraphy, and paleoclimate at the late Miocene Coffee Ranch fossil site in the Texas Panhandle, Palaeogeography Palaeoclimatology Palaeoecology, 485, 361-376.
Ma, W. W., M. X. Zhu, G. P. Yang, and T. Li (2018), Iron geochemistry and organic carbon preservation by iron (oxyhydr)oxides in surface sediments of the East China Sea and the south Yellow Sea, Journal of Marine Systems, 178, 62-74.
Ma, X. X., G. D. Zheng, W. Sajjad, W. Xu, Q. H. Fan, J. J. Zheng, and Y. Q. Xia (2018), Influence of minerals and iron on natural gases generation during pyrolysis of type-III kerogen, Marine and Petroleum Geology, 89, 216-224.
Maghfouri, S., M. R. Hosseinzadeh, A. Rajabi, and F. Choulet (2018), A review of major non-sulfide zinc deposits in Iran, Geoscience Frontiers, 9(1), 249-272.
Makvandi, S., G. Beaudoin, M. B. McClenaghan, and D. Quirt (2017), Geochemistry of magnetite and hematite from unmineralized bedrock and local till at the Kiggavik uranium deposit: Implications for sediment provenance, Journal of Geochemical Exploration, 183, 1-21.
Martin, A. P., C. Ohneiser, R. E. Turnbull, D. T. Strong, and S. Demler (2018), Soil magnetic susceptibility mapping as a pollution and provenance tool: an example from southern New Zealand, Geophysical Journal International, 212(2), 1225-1236.
Moska, P., G. Adamiec, Z. Jary, A. Bluszcz, G. Poreba, N. Piotrowska, M. Krawczyk, and J. Skurzynski (2018), luminescence chronostratigraphy for the loess deposits in Zlota, P
oland, Geochronometria, 45(1), 44-55.
Pan, D. D., T. Chen, Q. Zhan, and Z. H. Wang (2017), Mineral magnetic properties of Holocene sediments in the subaqueous Yangtze delta and the implications for human activity and early diagenesis, Quaternary International, 459, 133-143.
Pechersky, D. M., A. Y. Kazanskii, G. P. Markov, V. A. Tselmovich, and A. A. Shchetnikov (2018), Unique phenomenon of the accumulation of terrestrial metal iron particles in lacustrine deposits: Zhombolok volcanic region, East Sayan, Izvestiya-Physics of the Solid Earth, 54(1), 106-120.
Pechersky, D. M., D. M. Kuzina, E. V. Ivanov, M. I. Kuz'min, D. K. Nurgaliev, and V. A. Tsel'movich (2017), Thermomagnetic analysis of native iron from the upper sedimentary horizons of Lake Baikal, section GC-99 (Posolskaya Bank), Russian Geology and Geophysics, 58(12), 1561-1569.
Peretyazhko, T. S., P. B. Niles, B. Sutter, R. V. Morris, D. G. Agresti, L. Le, and D. W. Ming (2018), Smectite formation in the presence of sulfuric acid: Implications for acidic smectite formation on early Mars, Geochimica Et Cosmochimica Acta, 220, 248-260.
Perez-Cruz, L., and J. Urrutia-Fucugauchi (2018), Magnetic mineral diagenesis in anoxic laminated sediments from the Southern Gulf of California, Studia Geophysica Et Geodaetica, 62(1), 115-138.
Sahoo, P. K., et al. (2017), Geochemical characterization of the largest upland lake of the Brazilian Amazonia: Impact of provenance and processes, Journal of South American Earth Sciences, 80, 541-558.
Sitoe, S. R., J. Risberg, E. Norstrom, and L. O. Westerberg (2017), Late Holocene sea-level changes and paleoclimate recorded in Lake Lungue, southern Mozambique, Palaeogeography Palaeoclimatology Palaeoecology, 485, 305-315.
Sun, J., B. J. Mailloux, S. N. Chillrud, A. van Geen, A. Thompson, and B. C. Bostick (2018), Simultaneously quantifying ferrihydrite and goethite in natural sediments using the method of standard additions with X-ray absorption spectroscopy, Chemical Geology, 476, 248-259.
Uzarowicz, L., M. Skiba, M. Leue, Z. Zagorski, A. Gasinski, and J. Trzcinski (2018), Technogenic soils (Technosols) developed from fly ash and bottom ash from thermal power stations combusting bituminous coal and lignite. Part II. Mineral transformations and soil evolution, Catena, 162, 255-269.
Wang, R., W. Z. Shi, X. Y. Xie, L. L. Wang, A. B. Busbey, W. Manger, and Z. M. Xia (2017), Hydrothermal indications of Early Cretaceous red beds in lacustrine successions, North Yellow Sea Basin, eastern China, Marine and Petroleum Geology, 88, 739-755.
Wang, X. Y., Z. M. Shi, Y. Shi, S. J. Ni, R. L. Wang, W. Xu, and J. Y. Xu (2018), Distribution of potentially toxic elements in sediment of the Anning River near the REE and V-Ti magnetite mines in the Panxi Rift, SW China, Journal of Geochemical Exploration, 184, 110-118.
Zhang, R., and J. S. Nie (2017), Goethite Concentration Variations in the Red Clay Sequence on the Chinese Loess Pla-

teau, Geochemistry Geophysics Geosystems, 18(11), 4179-4185.

High Pressure and Extraterrestrial Magnetism

Artemieva, N., J. Morgan, and P. Expedition 364 Sci (2017), Quantifying the Release of Climate-Active Gases by Large Meteorite Impacts With a Case Study of Chicxulub, Geophysical Research Letters, 44(20), 10180-10188.

Badyukov, D. D., N. S. Bezaeva, P. Rochette, J. Gattacceca, J. M. Feinberg, M. Kars, R. Egli, J. Raitala, and D. M. Kuzina (2018), Experimental shock metamorphism of terrestrial basalts: Agglutinate-like particle formation, petrology, and magnetism, Meteoritics & Planetary Science, 53(1), 131-150.

Barth, M. I. F., D. Harries, F. Langenhorst, and P. Hoppe (2018), Sulfide-oxide assemblages in Acfer 094Clues to nebular metal-gas interactions, Meteoritics & Planetary Science, 53(2), 187-203.

Bell, M. S. (2017), Experimental shock decomposition of siderite and the origin of magnetite in martian meteorite Allan Hills 84001, Meteoritics & Planetary Science, 52, A21-A21.

Chemtob, S. M., R. D. Nickerson, R. V. Morris, D. G. Agresti, and J. G. Catalano (2017), Oxidative Alteration of Ferrous Smectites and Implications for the Redox Evolution of Early Mars, Journal of Geophysical Research-Planets, 122(12), 2469-2488.

Dunn, T. L., and J. Gross (201`7), Reclassification of Hart and Northwest Africa 6047: Criteria for distinguishing between CV and CK3 chondrites, Meteoritics & Planetary Science, 52(11), 2412-2423.

Evans, A. J., S. M. Tikoo, and J. C. Andrews-Hanna (2018), The Case Against an Early Lunar Dynamo Powered by Core Convection, Geophysical Research Letters, 45(1), 98-107.

Gemelli, M., T. Di Rocco, L. Folco, and M. D'Orazio (2017), Parentage Identification of Differentiated Achondritic Meteorites by Hand-held Energy Dispersive X-Ray Fluorescence Spectrometry, Geostandards and Geoanalytical Research, 41(4), 613-632.

Haberle, C. W., and L. A. J. Garvie (2017), Extraterrestrial formation of oldhamite and portlandite through thermal metamorphism of calcite in the Sutter's Mill carbonaceous chondrite, American Mineralogist, 102(12), 2415-2421.

Howarth, G. H., A. Udry, and J. M. D. Day (2018), Petrogenesis of basaltic shergottite Northwest Africa 8657: Implications for fO(2) correlations and element redistribution during shock melting in shergottites, Meteoritics & Planetary Science, 53(2), 249-267.

Kita, N. T., C. Defouilloy, C. A. Goodrich, and M. E. Zolensky (2017), oxygen isotope ratios of magnetite in ci-like clasts from a polymict ureilite, Meteoritics & Planetary Science, 52, A166-A166.

Lehner, S. W., P. Nemeth, M. I. Petaev, and P. R. Buseck (2017), Porous, S-bearing silica in metal-sulfide nodules and in the interchondrule clastic matrix in two EH3 chondrites, Meteoritics & Planetary Science, 52(11), 2424-2436.

Lewis, J. M. T., J. Najorka, J. S. Watson, and M. A. Sephton (2018), The Search for Hesperian Organic Matter on Mars: Pyrolysis Studies of Sediments Rich in Sulfur and Iron, Astrobiology.

Oliveira, J. S., M. A. Wieczorek, and G. Kletetschka (2017), Iron Abundances in Lunar Impact Basin Melt Sheets From Orbital Magnetic Field Data, Journal of Geophysical Research-Planets, 122(12), 2429-2444.

Rose, I., and B. Buffett (2017), Scaling rates of true polar wander in convecting planets and moons, Physics of the Earth and Planetary Interiors, 273, 1-10.

Schrader, D. L., and T. J. Zega (2017), microstructure of a pyrrhotite-pentlandite intergrowth in ll6 saint-severin, Meteoritics & Planetary Science, 52, A311-A311.

Fundamental Rock and Mineral Magnetism

Ferre, E. C., et al. (2017), Earthquakes in the Mantle? Insights From Rock Magnetism of Pseudotachylytes, Journal of Geophysical Research-Solid Earth, 122(11), 8769-8785.

Gaucher, F. E. S., and R. S. Smith (2017), The impact of magnetic viscosity on time-domain electromagnetic data from iron oxide minerals embedded in rocks at Opemiska, Quebec, Canada, Geophysics, 82(5), B165-B176.

Kletetschka, G., and M. A. Wieczorek (2017), Fundamental relations of mineral specific magnetic carriers for paleointensity determination, Physics of the Earth and Planetary Interiors, 272, 44-49.

Kosterov, A. A., E. S. Sergienko, P. V. Kharitonskii, and S. Y. Yanson (2018), Low temperature magnetic properties of basalts containing near similar to TM30 titanomagnetite, Izvestiya-Physics of the Solid Earth, 54(1), 134-149.

Newell, A. J. (2017), Frequency dependence of susceptibility in magnets with uniaxial and triaxial anisotropy, Journal of Geophysical Research-Solid Earth, 122(10), 7544-7561.

Roberts, A. P., T. P. Almeida, N. S. Church, R. J. Harrison, D. Heslop, Y. L. Li, J. H. Li, A. R. Muxworthy, W. Williams, and X. Zhao (2017), Resolving the Origin of Pseudo-Single Domain Magnetic Behavior, Journal of Geophysical Research-Solid Earth, 122(12), 9534-9558.

Sangode, S. J., M. Venkateshwarulu, R. Mahajan, and V. Randive (2017), Magnetic Mineralogical Variability along Deccan Trap Basalt Borehole (KBH07), Koyna Deep Continental Drilling Program, Western Maharashtra, India, Journal of the Geological Society of India, 90(6), 769-775.

Valdez-Grijalva, M. A., L. Nagy, A. R. Muxworthy, W. Williams, and K. Fabian (2018), The magnetic structure and palaeomagnetic recording fidelity of sub-micron greigite (Fe3S4), Earth and Planetary Science Letters, 483, 76-89.

Villaseca, C., V. C. Ruiz-Martinez, and C. Perez-Soba (2017), Magnetic susceptibility of Variscan granite-types of the Spanish Central System and the redox state of magma, Geologica Acta, 15(4), 379-+.

Geomagnetism

Buffett, B., and A. Puranam (2017), Constructing stochastic models for dipole fluctuations from paleomagnetic observations, Physics of the Earth and Planetary Interiors, 272, 68-77.

Irrgang, C., J. Saynisch-Wagner, and M. Thomas (2018), Depth of origin of ocean-circulation-induced magnetic signals, Annales Geophysicae, 36(1), 167-180.

Lund, S., D. Oppo, and W. Curry (2017), Late Quaternary paleomagnetic secular variation recorded in deep-sea sediments from the Demerara Rise, equatorial west Atlantic Ocean, Physics of the Earth and Planetary Interiors, 272, 17-26.

Simon, Q., D. L. Bourles, N. Thouveny, C. S. Horng, J. P. Valet, F. Bassinot, and S. Choy (2018), Cosmogenic signature of geomagnetic reversals and excursions from the Reunion event to the Matuyama-Brunhes transition (0.7-2.14 Ma interval), Earth and Planetary Science Letters, 482, 510-524.

Starchenko, S. V. (2017), Energy geodynamo parameters compatible with analytical, numerical, paleomagnetic models and observations, Izvestiya-Physics of the Solid Earth, 53(6), 908-921.

Magnetic Fabrics and Anisotropy

Biedermann, A. R., and S. A. McEnroe (2017), Effects of Magnetic Anisotropy on Total Magnetic Field Anomalies, Journal of Geophysical Research-Solid Earth, 122(11), 8628-8644.

Cheadle, M. J., and J. S. Gee (2017), Quantitative Textural Insights into the Formation of Gabbro in Mafic Intrusions, Elements, 13(6), 409-414.

Hrouda, F., and S. W. Faryad (2017), Magnetic fabric overprints in multi-deformed polymetamorphic rocks of the Gemeric Unit (Western Carpathians) and its tectonic implications, Tectonophysics, 717, 83-98.

Petri, B., E. Skrzypek, G. Mohn, T. Mateeva, P. Robion, K. Schulmann, G. Manatschal, and O. Muntener (2018), Mechanical anisotropies and mechanisms of mafic magma ascent in the middle continental crust: The Sondalo magmatic system (N Italy), Geological Society of America Bulletin, 130(1-2), 331-352.

Raposo, M. I. B. (2017), Magnetic fabrics of the Cretaceous dike swarms from Sao Paulo coastline (SE Brazil): Its relationship with South Atlantic Ocean opening, Tectonophysics, 721, 395-414.

Xue, Z. H., G. Martelet, W. Lin, M. Faure, Y. Chen, W. Wei, S. J. Li, and Q. C. Wang (2017), Mesozoic Crustal Thickening of the Longmenshan Belt (NE Tibet, China) by Imbrication of Basement Slices: Insights From Structural Analysis, Petrofabric and Magnetic Fabric Studies, and Gravity Modeling, Tectonics, 36(12), 3110-3134.

Zaffarana, C. B., R. Somoza, D. L. Orts, R. Mercader, B. Boltshauser, V. R. Gonzalez, and C. Puigdomenech (2017), Internal structure of the Late Triassic Central Patagonian batholith at Gastre, southern Argentina: Implications for pluton emplacement and the Gastre fault system, Geosphere, 13(6), 1973-1992.

Mineralogy, Petrology, Mineral Physics and Chemistry

Berry, A. J., G. A. Stewart, H. S. C. O'Neill, G. Mallmann, and J. F. W. Mosselmans (2018), A re-assessment of the oxidation state of iron in MORB glasses, Earth and Planetary Science Letters, 483, 114-123.

Broughm, S. G., J. M. Hanchar, F. Tornos, A. Westhues, and S. Attersley (2017), Mineral chemistry of magnetite from magnetite-apatite mineralization and their host rocks: examples from Kiruna, Sweden, and El Laco, Chile, Mineralium Deposita, 52(8), 1223-1244.

Paleointensity

Cai, S., L. Tauxe, and G. Cromwell (2017), Paleointensity From Subaerial Basaltic Glasses From the Second Hawaii Scientific Drilling Project (HSDP2) Core and Implications for Possible Bias in Data From Lava Flow Interiors, Journal of Geophysical Research-Solid Earth, 122(11), 8664-8674.

Di Chiara, A., A. R. Muxworthy, R. I. F. Trindade, and F. Bispo-Santos (2017), Paleoproterozoic Geomagnetic Field Strength From the Avanavero Mafic Sills, Amazonian Craton, Brazil, Geochemistry Geophysics Geosystems, 18(11), 3891-3903.

Sakuramoto, Y., T. Yamazaki, K. Kimoto, Y. Miyairi, J. Kuroda, Y. Yokoyama, and H. Matsuzaki (2017), A Geomagnetic Paleointensity Record of 0.6 to 3.2Ma From Sediments in the Western Equatorial Pacific and Remanent Magnetization Lock-In Depth, Journal of Geophysical Research-Solid Earth, 122(10), 7525-7543.

Paleomagnetism

Agarwal, A., L. M. Alva-Valdivia, M. L. Rivas-Sanchez, E. Herrero-Bervera, J. Urrutia-Fucugauchi, and V. Espejel-Garcia (2017), Emplacement dynamics and hydrothermal alteration of the Atengo ignimbrite, southern Sierra Madre Occidental, northwestern Mexico, Journal of South American Earth Sciences, 80, 559-568.

Barnett-Moore, N., E. Font, and M. Neres (2017), A Reply to the Comment on "Assessing Discrepancies Between Previous Plate Kinematic Models of Mesozoic Iberia and Their Constraints" by Barnett-Moore Et Al, Tectonics, 36(12), 3286-3297.

Calvin, P., J. J. Villalain, A. M. Casas-Sainz, L. Tauxe, and S. Torres-Lopez (2017), pySCu: A new python code for analyzing remagnetizations directions by means of small circle utilities, Computers & Geosciences, 109, 32-42.

Calvin, P., V. C. Ruiz-Martinez, J. J. Villalain, A. M. Casas-Sainz, and B. Moussaid (2017), Emplacement and Deformation of Mesozoic Gabbros of the High Atlas (Morocco): Paleomagnetism and Magnetic Fabrics, Tectonics, 36(12), 3012-3037.

Cao, Y., Z. M. Sun, H. B. Li, J. L. Pei, W. Xu, J. W. Pan, L. Zhang, X. Z. Ye, B. C. Huang, and Z. X. Wang (2017), New Early and Late Carboniferous paleomagnetic results from the Qaidam Block, NW China: Implications for the paleogeography of Central Asia, Tectonophysics, 717, 242-252.

Cifuentes-Nava, G., A. Goguitchaichvili, H. Lopez-Loera, M. Cervantes, A. Cortes, L. Sanchez-Bettucci, J. L. Macias, J. Morales, and J. Rosas-Elguera (2017), Full vector magnetic dating of some pyroclastic rocks associated to the Colima volcano, western Mexico, Boletin De La Sociedad Geologica Mexicana, 69(3), 577-590.

Conte, A. M., S. Cuccuru, M. D'Antonio, S. Naitza, G. Oggiano, F. Secchi, L. Casini, and F. Cifelli (2017), The post-collisional late Variscan ferroan granites of southern Sardinia (Italy): Inferences for inhomogeneity of lower crust, Lithos, 294, 263-282.

Fetisova, A. M., R. V. Veselovskiy, F. Scholze, and Y. P. Balabanov (2018), The new Permian-Triassic paleomagnetic pole for the East European Platform corrected for inclination shallowing, Izvestiya-Physics of the Solid Earth, 54(1), 150-162.

Gao, L., Z. Y. Yang, Y. B. Tong, H. Wang, C. Z. An, and H. F. Zhang (2017), Cenozoic clockwise rotation of the Chuan Dian Fragment, southeastern edge of the Tibetan Plateau: Evidence from a new paleomagnetic study, Journal of Geodynamics, 112, 46-57.

Halpin, J. A., N. R. Daczko, M. E. Kohler, and J. M. Whittaker (2017), Strike-slip tectonics during the Neoproterozoic-Cambrian assembly of East Gondwana: Evidence from a newly discovered microcontinent in the Indian Ocean (Batavia Knoll), Gondwana Research, 51, 137-148.

Iosifidi, A. G., V. A. Mikhailova, V. V. Popov, E. S. Sergienko, A. V. Danilova, and N. M. Otmas (2018), The Carboniferous of the Moscow syneclise: Paleomagnetic data, Izvestiya-Physics of the Solid Earth, 54(1), 163-177.

Jiang, Z. X., Q. S. Liu, M. J. Dekkers, X. Zhao, A. P. Roberts, Z. Y. Yang, C. S. Jin, and J. X. Liu (2017), Remagnetization mechanisms in Triassic red beds from South China, Earth and Planetary Science Letters, 479, 219-230.

Jing, X. Q., Z. Y. Yang, Y. B. Tong, H. Wang, and Y. C. Xu (2018), Identification of multiple magnetizations of the Ediacaran strata in South China, Geophysical Journal International, 212(1), 54-75.

Kirscher, U., V. Bachtadse, A. V. Mikolaichuk, A. Kroner, and D. V. Alexeiev (2017), Palaeozoic evolution of the North

Tianshan based on palaeomagnetic data - transition from Gondwana towards Pangaea, International Geology Review, 59(16), 2003-2020.
Ma, Y. M., et al. (2017), Paleomagnetic and Geochronologic Results of Latest Cretaceous Lava Flows From the Lhasa Terrane and Their Tectonic Implications, Journal of Geophysical Research-Solid Earth, 122(11), 8786-8809.
Mahgoub, A. N., H. Bohnel, C. Siebe, S. Salinas, and M. N. Guilbaud (2017), Paleomagnetically inferred ages of a cluster of Holocene monogenetic eruptions in the Tacambaro-Puruaran area (Michoacan, Mexico): Implications for volcanic hazards, Journal of Volcanology and Geothermal Research, 347, 360-370.
McNabb, J. C., R. J. Dorsey, B. A. Housen, C. W. Dimitroff, and G. T. Messe (2017), Stratigraphic record of Pliocene-Pleistocene basin evolution and deformation within the Southern San Andreas Fault Zone, Mecca Hills, California, Tectonophysics, 719, 66-85.
Meert, J. G., and M. Santosh (2017), The Columbia supercontinent revisited, Gondwana Research, 50, 67-83.
Meert, J. G., M. K. Pandit, A. Pivarunas, K. Katusin, and A. K. Sinha (2017), India and Antarctica in the Precambrian: a brief analysis, in Crustal Evolution of India and Antarctica: The Supercontinent Connection, edited by N. C. Pant and S. Dasgupta, pp. 339-351.
Merdith, A. S., et al. (2017), A full-plate global reconstruction of the Neoproterozoic, Gondwana Research, 50, 84-134.
Metelkin, D. V., A. I. Chernova, V. A. Vernikovsky, and N. Y. Matushkin (2017), Early Paleozoic Tectonics for the New Siberian Islands Terrane (Eastern Arctic), Doklady Earth Sciences, 477(1), 1277-1281.
Nonn, C., S. Leroy, K. Khanbari, and A. Ahmed (2017), Tectono-sedimentary evolution of the eastern Gulf of Aden conjugate passive margins: Narrowness and asymmetry in oblique rifling context, Tectonophysics, 721, 322-348.
Pastor-Galan, D., G. Gutierrez-Alonso, M. J. Dekkers, and C. G. Langereis (2017), Paleomagnetism in Extremadura (Central Iberian zone, Spain) Paleozoic rocks: extensive remagnetizations and further constraints on the extent of the Cantabrian orocline, Journal of Iberian Geology, 43(4), 583-600.
Pinton, A., G. Giordano, F. Speranza, and T. Thordarson (2018), Paleomagnetism of Holocene lava flows from the Reykjanes Peninsula and the Tungnaa lava sequence (Iceland): implications for flow correlation and ages, Bulletin of Volcanology, 80(1).
Piper, J. D. A. (2018), Dominant Lid Tectonics behaviour of continental lithosphere in Precambrian times: Palaeomagnetism confirms prolonged quasi-integrity and absence of supercontinent cycles, Geoscience Frontiers, 9(1), 61-89.
Qiao, Q. Q., B. C. Huang, A. J. Biggin, and J. D. A. Piper (2017), Late Cenozoic evolution in the Pamir-Tian Shan convergence: New chronological constraints from the magnetostratigraphic record of the southwestern Tianshan foreland basin (Ulugqat area), Tectonophysics, 717, 51-64.
Riel, N., E. Jaillard, J. E. Martelat, S. Guillot, and J. Braun (2018), Permian-Triassic Tethyan realm reorganization: Implications for the outward Pangea margin, Journal of South American Earth Sciences, 81, 78-86.
Rivera, T. A., R. Darata, P. C. Lippert, B. R. Jicha, and M. D. Schmitz (2017), The duration of a Yellowstone super-eruption cycle and implications for the age of the Olduvai subchron, Earth and Planetary Science Letters, 479, 377-386.
Sani, F., M. Ghinassi, M. Papini, O. Oms, and A. Finotello (2017), Evolution of the northern tip of Afar triangle: Inferences from the Quaternary succession of the Dandiero - Massawa area (Eritrea), Tectonophysics, 717, 339-357.
Subbarao, K. V., and V. Courtillot (2017), Deccan Basalts in and around Koyna - Warna Region, Maharashtra: Some Reflections, Journal of the Geological Society of India, 90(6), 653-662.
Thompson, M. D., J. Ramezani, and A. M. Grunow (2018), Within-Plate Setting of Paleozoic Alkalic Suites in Southeastern New England, USA: Constraints from Chemical Abrasion-TIMS U-Pb Geochronology and Paleomagnetism, Journal of Geology, 126(1), 41-61.
Usapkar, A., P. Dewangan, A. Mazumdar, K. S. Krishna, T. Ramprasad, F. K. Badesab, M. Patil, and V. V. Gaikwad (2018), Paleomagnetic record for the past 80 ka from the Mahanadi basin, Bay of Bengal, Journal of Asian Earth Sciences, 151, 226-239.
van der Boon, A., D. J. J. van Hinsbergen, M. Rezaeian, D. Gurer, M. Honarmand, D. Pastor-Galan, W. Krijgsman, and C. G. Langereis (2018), Quantifying Arabia-Eurasia convergence accommodated in the Greater Caucasus by paleomagnetic reconstruction, Earth and Planetary Science Letters, 482, 454-469.
van Hinsbergen, D. J. J., W. Spakman, R. L. M. Vissers, and D. G. van der Meer (2017), Comment on "Assessing Discrepancies Between Previous Plate Kinematic Models of Mesozoic Iberia and Their Constraints" by Barnett-Moore Et Al, Tectonics, 36(12), 3277-3285.
Veselovskiy, R. V., A. A. Arzamastsev, V. A. Tselmovich, A. M. Fetisova, and E. P. Kulakova (2017), Paleomagnetism of Precambrian dikes in the Kola part of northeastern Fennoscandia and its relation to the Svecofennian orogeny, Izvestiya-Physics of the Solid Earth, 53(6), 898-907.
Vizan, H., C. B. Prezzi, S. E. Geuna, M. S. Japas, E. M. Renda, J. Franzese, and M. A. Van Zele (2017), Paleotethys slab pull, self-lubricated weak lithospheric zones, poloidal and toroidal plate motions, and Gondwana tectonics, Geosphere, 13(5), 1541-1554.
Yalikun, Y., C. J. Xue, and D. T. A. Symons (2018), Paleomagnetic age and tectonic constraints on the genesis of the giant Jinding Zn-Pb deposit, Yunnan, China, Mineralium Deposita, 53(2), 245-259.
Yang, R. S., X. M. Fang, Q. Q. Meng, J. B. Zan, W. L. Zhang, T. Deng, Y. B. Yang, X. B. Ruan, L. Y. Yang, and B. S. Li (2017), Paleomagnetic Constraints on the Middle Miocene-Early Pliocene Stratigraphy in the Xining Basin, NE Tibetan Plateau, and the Geologic Implications, Geochemistry Geophysics Geosystems, 18(11), 3741-3757.

Prospecting and Surveying

Barnoud, A., C. Bouligand, O. Coutant, and J. Carlut (2017), Magnetic structure of Basse-Terre volcanic island (Guadeloupe, Lesser Antilles) inferred from 3D inversion of aeromagnetic data, Journal of Volcanology and Geothermal Research, 348, 1-11.
Cheng, W. B. (2018), Seismic evidence for central Taiwan magnetic low and deep-crustal deformation caused by plate collision, Journal of Asian Earth Sciences, 151, 334-342.
Fullea, J. (2017), On Joint Modelling of Electrical Conductivity and Other Geophysical and Petrological Observables to Infer the Structure of the Lithosphere and Underlying Upper Mantle, Surveys in Geophysics, 38(5), 963-1004.
Macnae, J. (2017), Superparamagnetism in ground and airborne electromagnetics: Geometrical and physical controls, Geophysics, 82(6), E347-E356.
Oerter, E., M. Singleton, and L. Davisson (2017), Hydrogen and oxygen stable isotope signatures of goethite hydration waters by thermogravimetry-enabled laser spectroscopy, Chemical Geology, 475, 14-23.
Patro, P. K. (2017), Magnetotelluric Studies for Hydrocarbon

and Geothermal Resources: Examples from the Asian Region, Surveys in Geophysics, 38(5), 1005-1041.
Ribeiro, J. A., F. A. Monteiro-Santos, M. F. Pereira, R. D. Fernandez, I. D. da Silva, C. Nascimento, and J. B. Silva (2017), Magnetotelluric Imaging of the Lithosphere Across the Variscan Orogen (Iberian Autochthonous Domain, NW Iberia), Tectonics, 36(12), 3065-3080.
Shi, Y. L., Z. X. He, Z. Z. Hu, Q. Wei, D. C. Li, C. X. Meng, L. S. Ji, and S. Zhang (2018), Mapping deep targets based on integrated 3D MT-gravity interpretation: a case study, Studia Geophysica Et Geodaetica, 62(1), 167-185.

Serpentinites

Klein, F., H. R. Marschall, S. A. Bowring, S. E. Humphris, and G. Horning (2017), Mid-ocean Ridge Serpentinite in the Puerto Rico Trench: from Seafloor Spreading to Subduction, Journal of Petrology, 58(9), 1729-1753.
Merkulova, M. V., M. Munoz, F. Brunet, O. Vidal, K. Hattori, D. Vantelon, N. Trcera, and T. Huthwelker (2017), Experimental insight into redox transfer by iron- and sulfur-bearing serpentinite dehydration in subduction zones, Earth and Planetary Science Letters, 479, 133-143.
Syverson, D. D., B. M. Tutolo, D. M. Borrok, and W. E. Seyfried (2017), Serpentinization of olivine at 300 degrees C and 500 bars: An experimental study examining the role of silica on the reaction path and oxidation state of iron, Chemical Geology, 475, 122-134.
Wojtulek, P. M., J. Puziewicz, and T. Ntaflos (2017), MORB melt metasomatism and deserpentinization in the peridotitic member of Variscan ophiolite: an example of the Braszowice-Brzeznica serpentinites (SW Poland), Journal of Geosciences, 62(3), 147-164.

Stratigraphy

Arkadiev, V. V., V. A. Grishchenko, A. Y. Guzhikov, A. G. Manikin, Y. N. Savelieva, A. A. Feodorova, and O. V. Shurekova (2017), Ammonites and magnetostratigraphy of the Berriasian-Valanginian boundary deposits from eastern Crimea, Geologica Carpathica, 68(6), 505-516.
De los Santos, M. G., T. F. Lawton, P. Copeland, A. Licht, and S. A. Hall (2018), Magnetostratigraphy, age and depositional environment of the Lobo Formation, southwest New Mexico: implications for the Laramide orogeny in the southern Rocky Mountains, Basin Research, 30, 401-423.
Duan, Z. Q., Q. S. Liu, C. C. Gai, and X. X. Zhao (2017), Magnetostratigraphic and environmental implications of greigite (Fe3S4) formation from Hole U1433A of the IODP Expedition 349, South China Sea, Marine Geology, 394, 82-97.
Gomez Samus, M. L., N. R. Chimento, J. Loffler, Y. Rico, L. Sierra, and J. Bidegain (2017), Neogene-Quaternary in Tandilia, South America: litho- bio- magnetostratigraphy, Journal of Iberian Geology, 43(4), 559-581.
Grappone, J. M., T. Chaffee, Y. Isozaki, H. Bauert, and J. L. Kirschvink (2017), Investigating the duration and termination of the Early Paleozoic Moyero Reversed Polarity Superchron: Middle Ordovician paleomagnetism from Estonia, Palaeogeography Palaeoclimatology Palaeoecology, 485, 673-686.
Rodelli, D., et al. (2018), High-resolution integrated magnetobiostratigraphy of a new middle Eocene section from the Neotethys (Elazig Basin, eastern Turkey), Geological Society of America Bulletin, 130(1-2), 193-207.
Sciscio, L., M. de Kock, E. Bordy, and F. Knoll (2017), Magnetostratigraphy across the Triassic-Jurassic boundary in the main Karoo Basin, Gondwana Research, 51, 177-192.
Turtu, A., V. Lauretano, R. Catanzariti, F. J. Hilgen, S. Galeotti, L. Lanci, M. Moretti, and L. J. Lourens (2017), Integrated stratigraphy of the Smirra Core (Umbria-Marche Basin, Apennines, Italy): A new early Paleogene reference section and implications for the geologic time scale, Palaeogeography Palaeoclimatology Palaeoecology, 487, 158-174.
van Peer, T. E., C. Xuan, P. C. Lippert, D. Liebrand, C. Agnini, and P. A. Wilson (2017), Extracting a Detailed Magnetostratigraphy From Weakly Magnetized, Oligocene to Early Miocene Sediment Drifts Recovered at IODP Site U1406 (Newfoundland Margin, Northwest Atlantic Ocean), Geochemistry Geophysics Geosystems, 18(11), 3910-3928.
Wu, F. L., X. M. Fang, Q. Q. Meng, Y. Zhao, F. J. Tang, T. Zhang, W. L. Zhang, and J. B. Zan (2017), Magneto- and litho-stratigraphic records of the Oligocene-Early Miocene climatic changes from deep drilling in the Linxia Basin, Northeast Tibetan Plateau, Global and Planetary Change, 158, 36-46.
Wu, H. C., M. N. Shi, X. X. Zhao, B. Y. Huang, S. H. Zhang, H. Y. Li, T. S. Yang, and C. S. Lin (2017), Magnetostratigraphy of ODP Site 1143 in the South China Sea since the Early Pliocene, Marine Geology, 394, 133-142.
Xu, Q. M., J. L. Yang, Y. Z. Hu, G. B. Yuan, and C. L. Deng (2018), Magnetostratigraphy of two deep boreholes in southwestern Bohai Bay: Tectonic implications and constraints on the ages of volcanic layers, Quaternary Geochronology, 43, 102-114.
Zhang, D. W., M. D. Yan, X. M. Fang, Y. B. Yang, T. Zhang, J. B. Zan, W. L. Zhang, C. L. Liu, and Q. Yang (2018), Magnetostratigraphic study of the potash-bearing strata from drilling core ZK2893 in the Sakhon Nakhon Basin, eastern Khorat Plateau, Palaeogeography Palaeoclimatology Palaeoecology, 489, 40-51.

The "fate rock" or "magnet mountain" which ruined every ship coming too close by pulling out all nails due to its terrible magnetic power 1.

cont'd. from pg. 1...

retain a remanence is due to thermal fluctuations, that change the magnetization too frequently within the timeframe of a measurement so that the magnetization is randomized. While these particles are not magnetic remanence carriers, they strictly belong to the group of single domain particles. However, what we think of when we talk about the single domain (SD) state, are particles that are slightly larger, i.e., the stable SD (SSD) state (Table 1). Rocks with high concentrations of SSD particles are what we look for, but rarely find. SSD particles are so highly sought after, as they are able to preserve records of magnetic fields for billions of years and we can use their remanence to understand the history of our solar system with them. As particles grow larger we approach a "grey area" of magnetic stability. Often referred to as 'pseudo single domain' (PSD), these grains have complex domain structures but can still be good recorders of the magnetic field. The name is somewhat disputed, as it makes no statement of the actual spin geometry, and "vortex state" is preferred by some. The final important size range encompasses the multidomain particles, which are typically magnetically soft (low B_c) and can easily be demagnetized. Therefore, the remanence stored in these grains is often unreliable. Natural rocks often contain a mixture of different magnetic minerals and different domain states, and determining the mineralogy as well as the domain state is important.

Whether the application is geared to paleomagnetic memory or material properties as indicators of past processes and conditions, rock-magnetic analysis is a critical part of the research. Here we want to provide a short overview of some of these methods, what their advantages are and how one may be able to use them to gain a better understanding of the magnetic carries in your samples. This is not a textbook and by no means a complete list, but we hope it will help you find the right method.

Often the easiest way to determine the size of something is to look at it. Technology is advancing rapidly, and we are now even able to look at individual atoms in a crystal. But often these methods are not directly applicable to rocks. The concentration of magnetite can be very low, so that just finding the particles of interest is often difficult. Superconducting Quantum Interference Device (SQUID) magnetometers, on the other hand, may still able to detect and measure the magnetic signal of a rock that contains a concentration of magnetite at the PPM level. Nonetheless, traditional imaging techniques, such as optical and electron microscopy are good ways to determine grain sizes. Working with synthetic powders is often easier, since you may be able to determine their size with Laser counters, through their Zeta potential or by means of X-Ray diffraction line broadening if the particles are < 100 nm. However, generally the particles in a rock are hidden in a matrix of non-magnetic material, that we are only partially interested in. Therefore, we need non-destructive methods that can estimate their size and/or their domain state.

Mineral	SP-SSD	SSD-MD	Reference
Magnetite (Fe_3O_4)	25-30 nm	50-60 nm	Dunlop (1973)
Hematite (Fe_2O_3)	25-30 nm	100 µm	Banerjee (1971); Kletetschka (2001)
Pyrrhotite (Fe_7S_8)		1.6 µm	Soffel (1977)

Table 1: Upper and lower limits for SSD state of different minerals at room temperature. These are highly variable and are strongly influenced by the shape of the particle.

A few concepts should be explained before we start. First, remanence ≠ remanence. There are several types of remanence, such as thermal remanence, isothermal remanence, anhysteretic remanence and many others. Without going into much detail on their acquisition (see Dunlop and Özdemir, 1997), they can be separated into two categories: remanences acquired in strong magnetic fields, usually applied in the lab; and weak-field remanences. Most natural processes belong to the second category. While their difference - the field strength - seems obvious, they create remanences that have vastly different properties (e.g. intensity, median destructive field). In the first part of this series, we will discuss tests that employ lab-induced strong-field remanences, as well as magnetization measured in the presence of strong applied fields. In future parts we will cover weak-field and thermal methods.

Strong-field tests

Hysteresis Loops (*HYS*): Hysteresis loops are among the most basic magnetic measurements (Ewing, 1885) but also the most fundamental. A hysteresis loop measures the magnetization of a sample in an applied field cycled to large positive and negative values, and can provide several important parameters. Firstly, the magnetization of ferrimagnetic materials reaches a limit $M(B\rightarrow\infty)$ called the saturation magnetization (M_s). M_s is a material constant for each mineral, and can be used to determine the concentration of ferromagnetic material in a sample. Usually the magnetic signal of bulk natural samples is a linear combination of ferri-, para- and diamagnetic signals and the high field slope (χ_{HF}) has to be corrected to isolate the ferrimagnetic signal, preferably using an approach-to-saturation technique (Fabian, 2006; Jackson and Sølheid, 2010). M_s is one of the few magnetic properties that is not grain-size dependent, at least above the nano-size range.

Secondly, the magnetization remaining when the field is zero is called remanent magnetization (M_r or M_{rs} if the sample was saturated). In contrast to M_s, the remanence is domain-state dependent in strength and stability. Note however, that the point at which the loop closes is generally significantly lower than that required for full saturation B_s. This can be called the field of remanence satura-

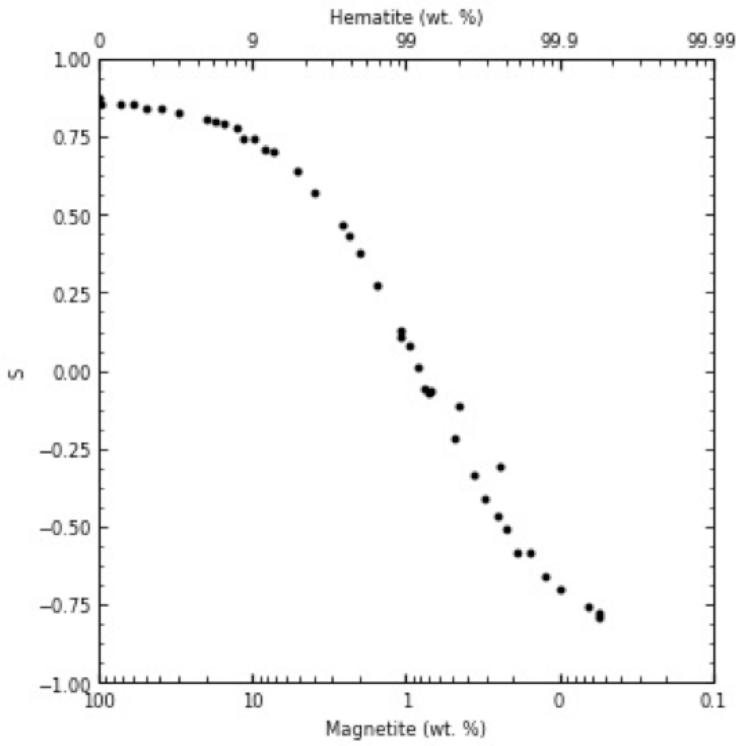

Figure 2: Classical *S*-ratio (-*M*(100 mT)/*SIRM*) for mixtures of synthetic magnetite and hematite. High *S*-ratios correspond to a Magnetite dominated sample, low values show hematite dominated sample. After Frank and Nowaczyk (2008).

tion B_{rs}, which for magnetite has a maximum value of ~240 kA/m or ~300 mT, where domains have all been driven out of the MD and PSD grains, and the magnetic moments of the stable single domain (SSD) particles that are present in the rock have all been non-reversibly turned in the polarity of the field. The nonlinear $M(B)$ regime between B_{rs} and B_s is the "approach to saturation," in which the individual-particle magnetic moments are forced to align parallel to the field, by rotating away from the particle long (easy) axes. Only when all the magnetic moments are parallel to the field M_s is obtained, and $M(B)$ thereafter becomes a line that increases indefinitely (if paramagnetic phases are present in the sample).

The field needed to achieve a zero net magnetization, while the field is applied, is the coercivity (B_c). Similar to M_r, B_c is also dependent on size. Large MD grains have smaller coercivities than SSD grains, since domain walls can be moved through a grain rather easily. Several other parameters are related to the magnetic mineralogy and particle-size distribution of the sample. Since most of the hysteresis parameters change as a function of grain-size, a simple hysteresis loop can already tell a lot about the nature of the magnetic carriers. Even mixtures of high- and low-coercivity materials can sometimes be determined by the shape of the loop (wasp-waisted, pot-bellied).

Keep in mind that your results are only as good as the measurement and proper calibration of the instrument, and that careful data processing (Jackson and Sølheid, 2010), is required to obtain reliable results, especially from weak samples. One example is the deconstruction of a loop into M_{ih} (induced hysteretic or reversible) and M_{rh} (remanent hysteretic or irreversible) components (von Dobeneck, 1996). These parts can be fitted with hyperbolic basis functions to reduce noise in weak samples, and to quantify the coercivity spectrum.

Direct Current Demagnetization Curves (*DCD*): These curves, often referred to as backfield curves, are used to determine the coercivity of remanence (B_{cr}) of a sample, and more generally to characterize the coercivity spectrum. After acquiring a saturation remanence, the sample is successively "demagnetized" in an increasingly stronger magnetic field with opposite polarity (i.e., the positive remanence is gradually replaced by a negative one, starting with the least coercive particles and proceeding through the coercivity spectrum). Figure 1 shows a major (fully saturated) hysteresis loop with several (A, B, C…) minor loops. On these minor loops, part of the remanence is recovered after the reverse field is switched off. Since a *DCD* is measured in a quasi-zero field and a hysteresis loop in an applied field, B_{cr} and B_c are generally different, with $B_{cr} \geq B_c$. Similar to the hysteresis parameters, B_{cr} is strongly dependent on the grain-size. In large grains $B_{cr} >> B_c$ while B_{cr} approaches the value of B_c in SSD particles. SP particles on the other hand, as they have no remanence, also have $B_{cr} = B_c = 0$. *DCD* measurements are generally more time consuming than *HYS*, and therefore several ways to estimate B_{cr} from a hysteresis loop have been proposed (Tauxe et al., 1996; Fabian and von Dobeneck, 1997; Fabian 2003). The simplest estimate is given by the median destructive field (*MDF*) of the remanent hysteretic part of the hysteresis (B_{rh}) .

Isothermal Remanent Magnetization (*IRM*) Acquisition Curves: *IRM* acquisition curves are related to the *DCD*. However, instead of "demagnetizing" (progressively reversing) the saturation magnetization, the measurement starts from a demagnetized state. Increasing magnetic fields are applied to acquire the *IRM*, which is measured step by step in a zero field. Since the initial magnetization should be zero, it is helpful to measure the *IRM* before the *DCD* curve. Natural rocks usually contain a number of different minerals, each with a distribution of sizes, and *IRM* acquisition curves (and their derivatives) can give information on the number of components present and their coercivity ranges (e.g., Dunlop, 1972). The overall magnetization is a superposition of the signals of the individual components and as such, can in certain cases be unmixed, assuming that the end-member contributions are linearly additive (Lees, 1997). In *IRM* unmixing (Robertson and France, 1994; Kruiver et al., 2001; Egli, 2003), the data are plotted against log(B) and fitted with analytical distribution functions. The function and pretreatment (e.g. filtering, interpolation) of the data depends on the means of calculation (excel spreadsheet, software, online applications (Maxbauer et al., 2016)). If many *IRM*s, or *DCD*s, are measured, the data can be unmixed without any a priori specification of the distribution functions that best rep-

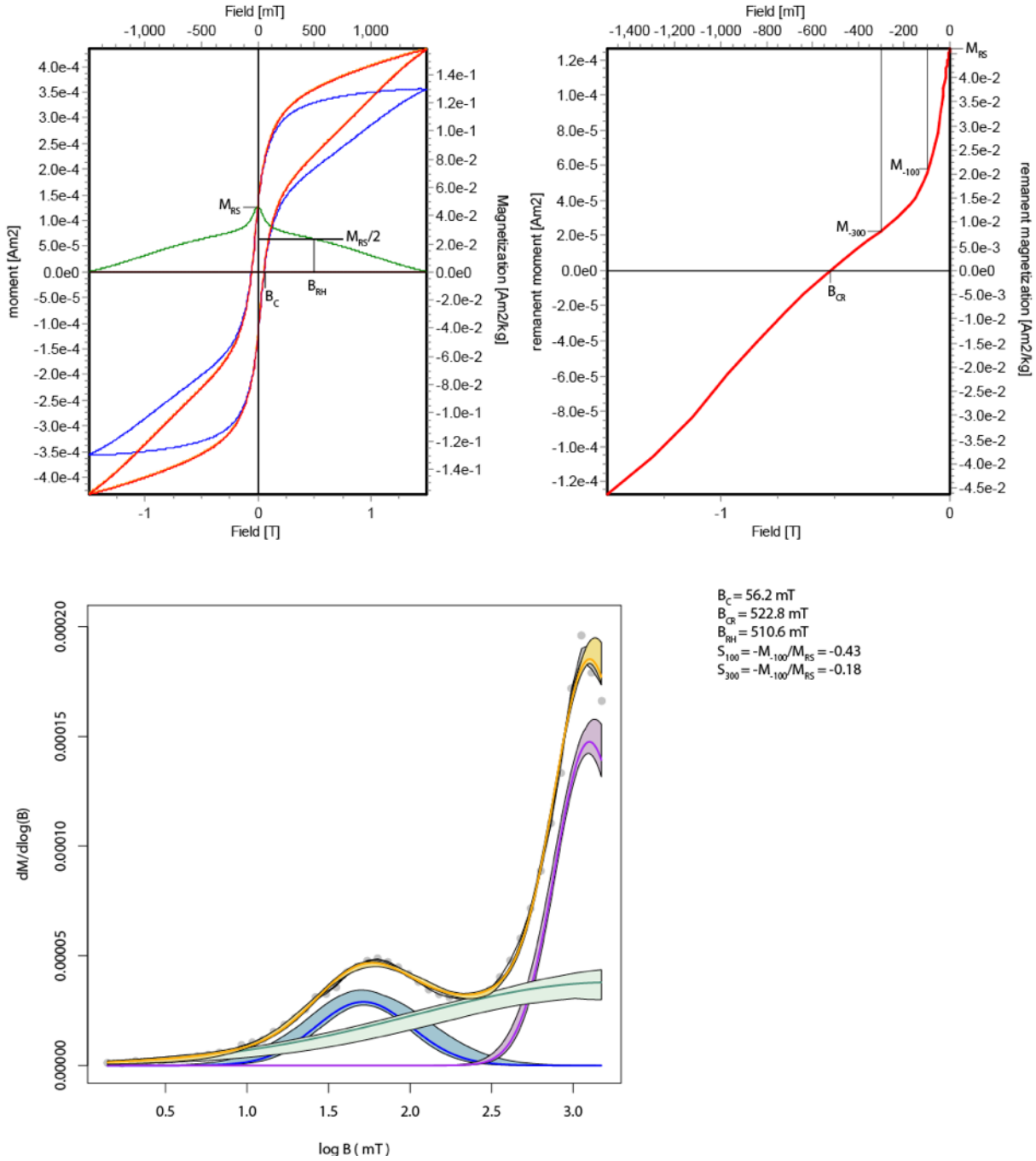

Figure 3: Hysteresis loop (red = raw data, blue = slope-corrected, green = M_{rh}), *DCD* curve, and coercivity spectrum unmixed using MAX UnMix (Maxbauer et al., 2016), for an obsidian from the Gutansar volcanic complex, Armenia, containing magnetite and hematite (Frahm et al., 2014). Loops and backfield curves clearly show at least two coercivity components; unmixing reveals a third broadly-distributed component (color bands show statistical uncertainty determined by resampling analysis).

resent the samples' components (e.g. Heslop and Dillon, 2007). The final output gives a mathematical description of the individual parts that, when combined, make up the rocks' magnetic signal.

These three types of measurements (*HYS*, *DCD* and *IRM*) are utilized in most paleomagnetic studies. There are several methods to further analyze the parameters determined from these that allow us to obtain a better understanding of the samples' domain state.

***S*-ratio:** In environmental magnetism, it is often useful to quantify, if only on a relative scale, the amounts of magnetic soft (e.g. magnetite) and hard (e.g. hematite) particles. In some cases, this can be estimated from the data of a *DCD* curve. The classical *S*-ratio is defined as the ratio of the moment at a given backfield (typically 300 mT) and the SIRM (i.e. M_r) (Stober and Thompson, 1979); $S = -M_{300\ mT}/SIRM$. Values can range from -1 to 1 representing the range from only high coercivity components (-1) to only low coercivity components (1), respectively (Fig.2). Other definitions have been used in the literature but the general idea is the same (Heslop, 2009). One problem with this approach, however is that substitutions in hematite (e.g. Al) can cause widely varying coercivities. In cases, where the hematite has an un-

usually low coercivity, it can cause an overestimation of the magnetite content.

***L*-ratio:** Another proposed parameter in environmental studies is the *L*-ratio (Liu et al., 2007), which, building from the *S*-ratio, provides a way of quantifying the concentration of high coercivity minerals (hematite, goethite). Here an *IRM* is acquired in a 1T field and *AF*-demagnetized in a 100 mT ($IRM_{AF100mT}$) and subsequently 300 mT field ($IRM_{AF300mT}$). The $IRM_{AF300mT}$ is often called hard *IRM* (*HIRM*) and can be used as a composition indicator on its own. However, in contrast to the *S*-ratio, the *L*-ratio ($IRM_{AF300mT}/IRM_{AF100mT}$) is thought to be independent of composition (Fe-substitutions). Most modern VSMs have the option to apply alternating magnetic fields (albeit at much lower frequencies than conventional *AF* instruments), and they allow a coarse *AF* demagnetization without requiring a specialized high field *AF*-coil.

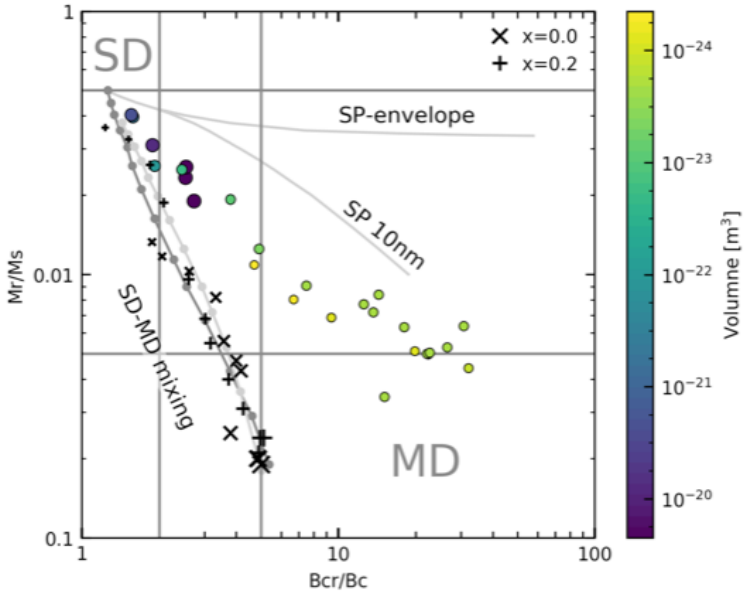

Figure 4: Day Plot of hysteresis data for two sample sets. Black markers show the data from Day et al. 1977 for Ti content x=0 (cross) and x=0.2 (plus) with marker size according to grain size. Colored circles represent samples of the Tiva Canyon Tuff, containing dominantly elongate SP-SSD titanomagnetite particles with narrow size distributions. TEM studies [Schlinger et al, 1991] give modal particle sizes ranging from 5.5x15 nm (~4.5x10-25 m^3) to 25x250 nm (~1.5x10-22 m^3). Markersize as well as color scale reflect the volume of the particles on a $\log_{10}$ scale.

Day Plot: The Day plot is probably one of the most widely used ways of plotting to evaluate the domain states of a set of samples. It was introduced by Day et al (1977), who measured hysteresis loops and backfield curves for titanomagnetite samples (TM) with a variety of compositions and particle sizes. They constructed different biparametric plots and found that when the remanence ratio (M_r/M_s) is plotted against the coercivity ratio (B_{cr}/B_c), a clear trend emerged that was mostly independent of TM composition, isolating the particle-size dependence. They defined SSD, PSD and MD regions, which indicate the overall domain state. Later Dunlop (2002a, 2002b) revisited the test and adjusted the boundaries. Furthermore, he determined how mixtures of SSD/MD and SP/SSD would influence the data and proposed the often cited mixing curves.

In particular, the remanence ratio has a theoretical justification. An assemblage of randomly oriented, non-interacting single domain particles with uniaxial anisotropy should have a value of 0.5 (Stoner and Wohlfarth, 1948). However, this value can change depending on the crystalline anisotropy and on the orientation distribution of the easy axes. Nonuniform magnetization states, and especially increasing domain multiplicity, cause M_r/M_s to

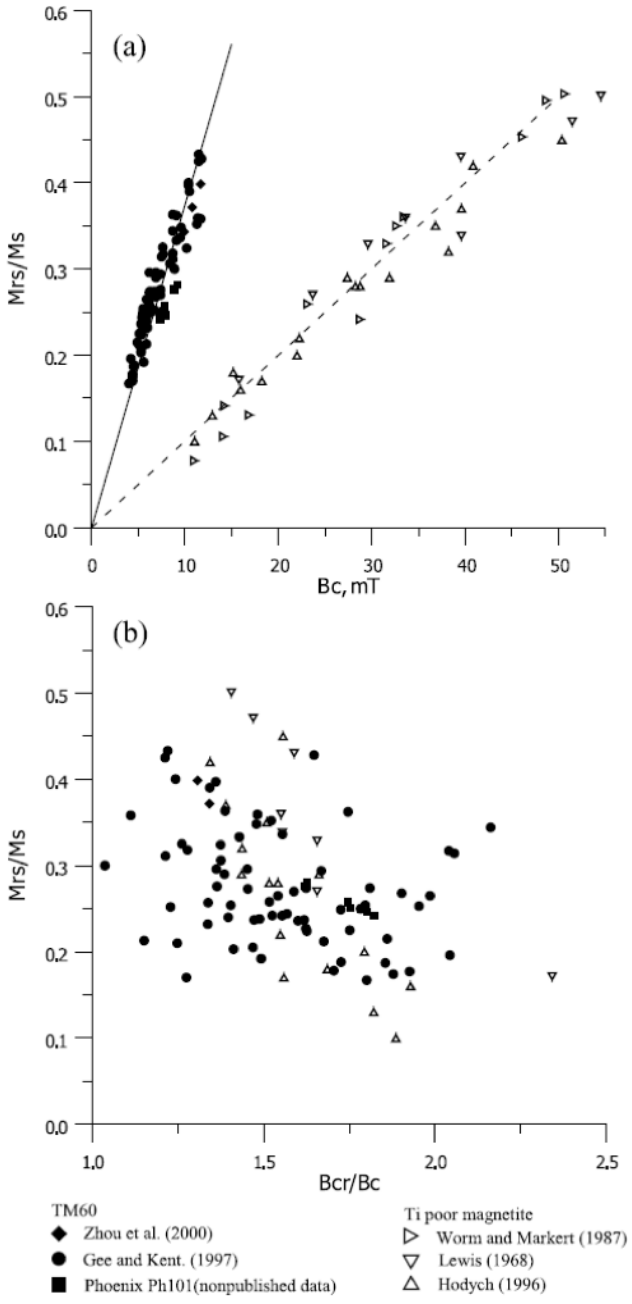

Figure 5: The "squareness-coercivity plot" (a) is sensitive to variations in magnetic grain size (domain state) and to Ti-content of the magnetite (Tauxe et al, 2002; Wang and Van der Voo, 2004), in contrast to the Day plot (b) which was designed to minimize (titano-) magnetite composition sensitivity and focus on particle sizes. Graphs from Wang and Van der Voo (2004).

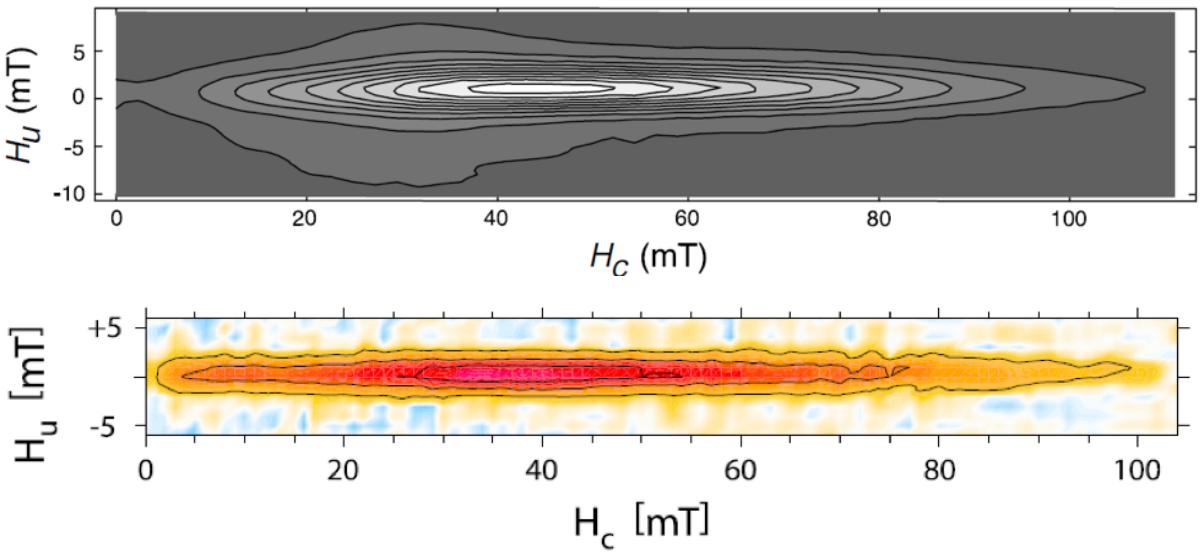

Figure 6: Room-temperature *FORC* distributions for (top) Tiva Canyon tuff sample CS911 containing non-interacting single-domain titanomagnetite particles (Pike et al., 2001) and (bottom) the "central ridge" of a high-resolution *FORC* diagram for a sediment sample from Lake Ely containing magnetotactic bacteria with intact chains of SSD magnetosomes (Egli et al., 2010).

decrease with increasing particle sizes.

While the Day plot appears to be an easy way to estimate domain state, it is not without controversy. The main issue with this simple interpretation of magnetic parameters is that it reduces the level of detail in a loop to a single point on the Day plot, for the purpose of easy comparison of large sample numbers, and much information is thereby discarded. There is also the fact that many factors can influence the data, and data often do not lie on the proposed mixing lines. For instance, the domain state regions were determined only for titanomagnetites. Other minerals may plot in the SD range but that does not necessarily mean that they are (see the compilation of different minerals in Peters and Dekkers, 2003). Consequently, samples don't necessarily plot in their designated regions and additional knowledge of the mineralogy of the sample is necessary.

Squareness-Coercivity plot: A predecessor of the Day plot is the squareness plot (Néel, 1955; Tauxe et al., 2002). Instead of plotting the squareness of the hysteresis loop (M_r/M_s) against the ratio of the coercivities, it is simply plotted against coercivity (fig. 4a). Both parameters are easily determined from a simple hysteresis plot, which avoids the extra *DCD* measurement. Because the coercivity depends on the composition, this method is not independent of the Ti-content of magnetite. The Day plot, on the other hand, is used exactly because of its relative independence to Ti content (fig. 4b). Consequently, the squareness-coercivity plot can not only be used to gain understanding on the domain state of samples but also indicates their composition. This, in combination with the Curie temperature, which for magnetite is strongly dependent on the Ti content, can be a useful addition to a study.

Preisach Methods: Simple hysteresis loops omit much of the magnetic information, which is stored in the transient hysteresis, the difference of ascending and descending hysteresis branches. Other, more sophisticated methods can use this information to better understand the domain-state. The Preisach model was originally derived as a mathematical description of the hysteretic processes of non SD materials (Preisach, 1935). As of today, several experimental approaches have been developed to understand these magnetization process.

The most common are the so-called first-order reversal curve diagrams (*FORC*, fig. 5). *FORC*s are a relatively new, increasingly popular method that allow for a visual interpretation of the distribution of domain states (Pike et al., 1999, Roberts et al. 2000). They are a modification of the simple hysteresis plot, but the measurement procedure is more complicated (see Roberts et al., 2014). The sample is saturated at the saturation field B_{sat}. Next, the field is ramped down to some reversal field B_r and the magnetization curve ($M(B_r, B)$) from B_r is measured while B increases; this is a single *FORC* curve. The process is repeated for a range of reversal fields, and depending on the field steps (B, B_r), a *FORC* data set can easily have more than 5000 individual measurements. A mixed derivative with respect to B_r and B is calculated and displayed as a contour plot. Several methods for calculating, correcting, and smoothing the data have been proposed, each with their own advantages (Vari*FORC* (Egli, 2013), *FORC*inel (Harrison and Feinberg, 2008)…).

A lesser-known, even more elaborate variety is the second order reversal curve (*SORC*). In general, the measurement procedure is similar to that of a *FORC*. However, a second reversal field B_{r2} is introduced and an extra magnetization curve $M(B_r, B_{r2}, B)$, that branches out from the *FORC* $M(B_r, B)$ curve is measured. The extra curves require even more measurements, making the procedure extremely time consuming, so that few *SORC*s have actually been measured (Winklhofer et al. 2008).

Preisach diagrams (e.g. Church et al. 2016) or remanent *FORC* diagrams (r*FORC*) (e.g. Bodale et al. 2011)

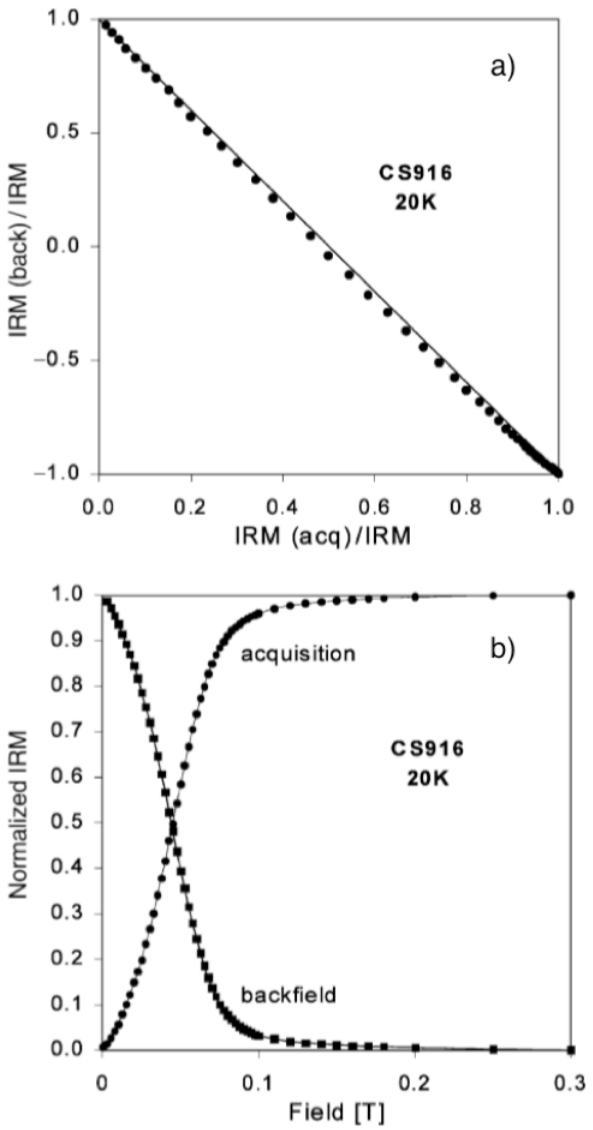

Figure 7: Henkel (a) and Cisowski (b) plots for a Tiva Canyon tuff sample at 20K, showing ideal non-interacting SSD behavior (Worm and Jackson, 1999).

are another method that is gaining popularity. They differ from *FORC*s and *SORC*s, as only the remanent magnetization is measured. Starting from a *SIRM*, a field with opposite polarity is applied, much like a *DCD*. From this somewhat demagnetized state, an *IRM* acquisition curve is measured.

Preisach methods are able to show features that are considered diagnostic of certain domain states. For example, a sample containing SSD grains will show a prominent central ridge along B_c, distinctly different from MD grains, that display a vertical distribution at B_c=0. Thus, they can help in the interpretation of single and mixed domain state samples (e.g. SD+MD), show evidence of thermal relaxation effects (Pike et al., 2001), and show interactions between particles (though we note here that certain groups of particles, e.g. the chains produced by magnetotactic bacteria, are so strongly interacting that they are equivalent to isolated, non-interacting SSD particles on a *FORC* diagram! See fig.5b). While a single well-measured FORC will lead to a better understanding of the magnetic state of an individual sample, large numbers of *FORC*s can be used to understand differences between samples, or the distribution of properties in a population of samples, using principal component analysis (Lascu, 2015). Similar to unmixing of *IRM*s, this method allows for the separation of the individual components of mixed state systems using a mathematical formalism. Therefore, common remanence carriers in the samples can be determined and their spatial or temporal variations analized.

However, all of these methods are much more time-consuming than typical *HYS*, *DCD*, *IRM* measurements and measurement times of several hours are normal, even with the help of special gridding techniques (Zhao et al. 2015). Ultimately, time is the price to pay for a better understanding of particle systems.

Henkel Plot: Assuming there are no interactions, which is a whole different kind of problem, the *IRM* acquisition curve should be easily relatable to the *DCD* curve (Wohlfarth, 1958). The backfield curve goes from M_r to $-M_r$, and the *IRM* from 0 - M_r. Therefore, the moment at a given field $M(B)_{DCD} = M_r - 2\,M(B)_{IRM}$. Henkel (1964) was the first to plot the *DCD* curve against the *IRM* acquisition and show a linear relationship. Thus if the sample contains purely SD particles without interactions, the Henkel plot returns a linear slope of -2 (fig. 6a).

Cisowski Test: Similar to the Henkel plot, the Cisowski (1981) test uses an IRM acquisition curve plotted together with an alternating field (*AF*) demagnetization of M_r (*SIRM*). If the point (*R*), at which the two normalized curves cross, has an ordinate value of 0.5 (i.e., the median acquisition field and *MDF* are equal (see Dankers, 1981)), the sample is dominated by non-interacting SD particles (fig. 6b). For obvious reasons this plot is often informally referred to as the crossover plot. This method was expanded on by Symons et al. (2000) for a variety of different mineralogies and therefore can also give information on the carrier minerals.

In many cases, to save time measuring the *AF* curve, the test is performed using an appropriately scaled *DCD* curve instead. Both the Henkel plot and Cisowski tests have in common that they show if the sample is in a stable non-interacting SD state. However, the tests can be somewhat misleading: if magnetostatic interactions are at play the tests also indicate non-SD behavior. On the other hand, these tests can provide a useful addition when making interpretations on a sample that has already shown predominantly SD behavior through other tests.

Most magnetic properties depend on the domain state and consequently particle size of the magnetic carrier-minerals of a rock. However, they are also heavily influenced by the mineralogy, so that other tests should be used to probe the mineral composition of the specimen. In this first installment, we have presented methods that use strong field magnetizations, and can be used to estimate the domain state of a specimen or suite of specimens. A multitude of other tests have also been estab-

lished over the years, many of which rely on weak field magnetizations, susceptibilities, or changing magnetic properties as a function of temperature. These tests will be discussed in subsequent articles. As a final word, keep in mind that no single test provides a definitive answer, so patience (and instrument-time) is key!

References

Banerjee, S.K. (1971) New Grain Size Limits for Palaeomagnetic Stability in Haematite. Nature Physical Science, 232, 15–16.

Bodale, I., Stoleriu, L., and Stancu, A. (2011) Reversible and Irreversible Components Evaluation in Hysteretic Processes Using First and Second-Order Magnetization Curves. IEEE Transactions on Magnetics, 47, 192–197.

Church, N.S., Fabian, K., and McEnroe, S.A. (2016) Nonlinear Preisach maps: Detecting and characterizing separate remanent magnetic fractions in complex natural samples. Journal of Geophysical Research: Solid Earth, 121, 8373–8395.

Cisowski, S.M. (1981) Interacting vs. non-interacting single domain behavior in natural and synthetic samples. Physics of the Earth and Planetary Interiors, 26, 56–62.

Dankers, P. H. M. (1981), Relationship between median destructive field and coercive forces for dispersed natural magnetite, titanomagnetite, and hematite, Geophys. J. R. Astr. Soc., 64, 447–461

Day, R. (1977) TRM and its variation with grain size. Journal of geomagnetism and geoelectricity, 29, 233–265.

Day, R., Fuller, M.D., and Schmidt, V.A. (1977) Hysteresis properties of titanomagnetites: Grain-size and compositional dependence. Physics of the Earth and Planetary Interiors, 13, 260–267.

Dobeneck, von, T. (1996) A systematic analysis of natural magnetic mineral assemblages based on modelling hysteresis loops with coercivity-related hyperbolic basis functions. Geophysical Journal International, 124, 675–694.

Dunlop, D. J. (1972), Magnetic mineralogy of unheated and heated red sediments by coercivity spectrum analysis, Geophys. J. R. Astr. Soc., 27, 37–55

Dunlop, D.J. (1973) Superparamagnetic and single-domain threshold sizes in magnetite. Journal of Geophysical Research, 78.

Dunlop, D.J. (2002a) Theory and application of the Day plot (Mrs/ Ms versus Hcr/ Hc) 1. Theoretical curves and tests using titanomagnetite data. Journal of Geophysical Research: Solid Earth, 107, 2056.

Dunlop, D.J. (2002b) Theory and application of the Day plot (Mrs/ Ms versus Hcr/ Hc) 2. Application to data for rocks, sediments, and soils. Journal of Geophysical Research: Solid Earth, 107, 2057.

Dunlop, D.J., and Özdemir, Ö. (1997) Rock Magnetism. Cambridge University Press, Cambridge.

Dunlop, D.J., Hanes, J.A., and Buchan, K.L. (1973) Indexes of Multidomain Magnetic Behavior in Basic Igneous Rocks - Alternating-Field Demagnetization, Hysteresis, and Oxide Petrology. Journal of Geophysical Research, 78, 1387–1393.

Egli, R. (2003) Analysis of the field dependence of remanent magnetization curves. Journal of Geophysical Research: Solid Earth, 108, 335.

Egli, R., A. P. Chen, M. Winklhofer, K. P. Kodama, and C.-S. Horng (2010), Detection of noninteracting single domain particles using first-order reversal curve diagrams, Geochem. Geophys. Geosyst., 11(1), Q01Z11, doi: 10.1029/2009gc002916.

Egli, R. (2013), VARIFORC: an optimized tool for the calculation of non-regular first order reversal curve (FORC) diagrams, Global Planet. Change, 110, 302-320, doi: 10.1016/j.gloplacha.2013.08.003.

Ewing, J.A. (1885) X. Experimental researches in magnetism. Philosophical Transactions of the Royal Society of London, 176, 523–640.

Fabian, K. (2003) Some additional parameters to estimate domain state from isothermal magnetization measurements. Earth and Planetary Science Letters, 213, 337–345.

Fabian, K. (2006) Approach to saturation analysis of hysteresis measurements in rock magnetism and evidence for stress dominated magnetic anisotropy in young mid-ocean ridge basalt. Physics of the Earth and Planetary Interiors, 154, 299–307.

Fabian, K., and Dobeneck, von, T. (1997) Isothermal magnetization of samples with stable Preisach function: A survey of hysteresis, remanence, and rock magnetic parameters. Journal of Geophysical Research: Solid Earth, 102, 17659–17677.

Frahm, E., J. M. Feinberg, B. A. Schmidt-Magee, K. Wilkinson, B. Gasparyan, B. Yeritsyan, S. Karapetian, K. Meliksetian, M. J. Muth, and D. S. Adler (2014), Sourcing geochemically identical obsidian: multiscalar magnetic variations in the Gutansar volcanic complex and implications for Palaeolithic research in Armenia, J. Archaeol. Sci, 47, 164-178, doi: 10.1016/j.jas.2014.04.015.

Frank, U., and Nowaczyk, N.R. (2008) Mineral magnetic properties of artificial samples systematically mixed from haematite and magnetite. Geophysical Journal International, 175, 449–461.

Gong, Z., Dekkers, M.J., Heslop, D., and Mullender, T.A.T. (2009) End-member modelling of isothermal remanent magnetization (IRM) acquisition curves: a novel approach to diagnose remagnetization. Geophysical Journal International, 178, 693–701.

Harrison, R. J., and J. M. Feinberg (2008), FORCinel: An improved algorithm for calculating first-order reversal curve distributions using locally weighted regression smoothing, Geochem. Geophys. Geosyst, 9(Q05016), doi:10.1029/2008GC001987

Henkel, O. (1964) Remanenzverhalten und Wechselwirkungen in hartmagnetischen Teilchenkollektiven. physica status solidi (b), 7, 919–929.

Heslop, D. (2009) On the statistical analysis of the rock magnetic S-ratio. Geophysical Journal International, 178, 159–161.

Heslop, D. (2015), Numerical strategies for magnetic mineral unmixing, Earth-Sci. Rev, 150, 256-284, doi: http://dx.doi.org/10.1016/j.earscirev.2015.07.007.

Heslop, D., and Dillon, M. (2007) Unmixing magnetic remanence curves without a priori knowledge. Geophysical Journal International, 170, 556–566.

Jackson, M.J., and Solheid, P.A. (2010) On the quantitative analysis and evaluation of magnetic hysteresis data. Geochemistry, Geophysics, Geosystems, 11, n/a–n/a.

Jackson, M.J., Gruber, W., Marvin, J., and Banerjee, S.K. (1988) Partial anhysteretic remanence and its anisotropy: Applications and grainsize-dependence. Geophysical Research Letters, 15, 440–443.

Kruiver, P.P., Dekkers, M.J., and Heslop, D. (2001) Quantification of magnetic coercivity components by the analysis of acquisition curves of isothermal remanent magnetisation. Earth and Planetary Science Letters.

Lascu, I., Harrison, R.J., Li, Y., Muraszko, J.R., Channell, J.E.T., Piotrowski, A.M., and Hodell, D.A. (2015) Magnetic unmixing of first-order reversal curve diagrams using

principal component analysis. Geochemistry, Geophysics, Geosystems, 16, 2900–2915.
Lees, J.A. (1997) Mineral magnetic properties of mixtures of environmental and synthetic materials: linear additivity and interaction effects. Geophysical Journal International, 131, 335–346.
Maxbauer, D.P., Feinberg, J.M., and Fox, D.L. (2016) MAX UnMix: A web application for unmixing magnetic coercivity distributions. Computers & Geosciences, 95, 140–145.
Néel, L. (1955). Some Theoretical Aspects of Rock-Magnetism. Adv. Phys, 4, 191–243.
Peters, C., and Dekkers, M.J. (2003) Selected room temperature magnetic parameters as a function of mineralogy, concentration and grain size. Physics and Chemistry of the Earth, Parts A/B/C, 28, 659–667.
Pike, C.R., Roberts, A.P., and Verosub, K.L. (1999) Characterizing interactions in fine magnetic particle systems using first order reversal curves. Journal of Applied Physics, 85, 6660–6667.
Preisach, F. (1935), Über die magnetische Nachwirkung, Z. Phys., 94, 277–302
Roberts, A.P., Cui, Y., and Verosub, K.L. (1995) Wasp-waisted hysteresis loops: Mineral magnetic characteristics and discrimination of components in mixed magnetic systems. Journal of Geophysical Research: Solid Earth, 100, 17909–17924.
Roberts, A.P., Heslop, D., Zhao, X., and Pike, C.R. (2014) Understanding fine magnetic particle systems through use of first-order reversal curve diagrams. Reviews of Geophysics, 52, 557–602.
Roberts, A.P., Pike, C.R., and Verosub, K.L. (2000) First-order reversal curve diagrams: A new tool for characterizing the magnetic properties of natural samples. Journal of Geophysical Research: Solid Earth, 105, 28461–28475.
Roberts, A.P., Pike, C.R., and Verosub, K.L. (2001) First-order reversal curve diagrams and thermal relaxation effects in magnetic particles. Geophysical Journal International, 145, 721–730.
Robertson, D.J., and France, D.E. (1994) Discrimination of remanence-carrying minerals in mixtures, using isothermal remanent magnetisation acquisition curves. Physics of the Earth and Planetary Interiors, 82, 223–234.
Schlinger, C. M., D. R. Veblen, and J. G. Rosenbaum (1991), Magnetism and magnetic mineralogy of ash flow tuffs from Yucca Mountain, Nevada, J. Geophys. Res. B, 96, 6035–6052
Soffel, H.C. (1977) Pseudo-Single-Domain Effects and Single-Domain Multidomain Transition in Natural Pyrrhotite Deduced From Domain-Structure Observations. Journal of Geophysics, 42, 351–359.
Stober, J.C., and Thompson, R. (1979) An investigation into the source of magnetic minerals in some Finnish lake sediments. Earth and Planetary Science Letters, 45, 464–474.
Stoner, E.C., and Wohlfarth, E.P. (1948) A mechanism of magnetic hysteresis in heterogeneous alloys. IEEE Transactions on Magnetics, 27, 3475–3518.
Symons, D.T.A., and Cioppa, M.T. (2000) Crossover plots: A useful method for plotting SIRM data in paleomagnetism. Geophysical Research Letters, 27, 1779–1782.
Tauxe, L., Mullender, T.A.T., and Pick, T. (1996) Potbellies, wasp-waists, and superparamagnetism in magnetic hysteresis. Journal of Geophysical Research: Solid Earth, 101, 571–583.
Tauxe, L., H. N. Bertram, and C. Seberino (2002), Physical interpretation of hysteresis loops: Micromagnetic modeling of fine particle magnetite, Geochem. Geophys. Geosyst., 3(10), 1-22, doi: 10.1029/2001GC000241.
Thompson, R., and Oldfield, F. (1986) Environmental Magnetism, 1 p. Springer NEtherlands.
Vérard, C., Leonhardt, R., Winklhofer, M., and Fabian, K. (2008) On the possibility of recovering palaeo-diurnal magnetic variations in transitional lava flows 2. An experimental case study. Physics of the Earth and Planetary Interiors, 169, 117–130.
Wang, D., and R. Van der Voo (2004), The hysteresis properties of multidomain magnetite and titanomagnetite/titanomaghemite in mid-ocean ridge basalts, Earth Planet. Sci. Lett., 220, 175-184
Worm, H.-U., and M. Jackson (1999), The superparamagnetism of Yucca Mountain Tuff, J. Geophys. Res. B, 104(B11), 25,415-425,425
Zhao, X., Heslop, D., and Roberts, A.P. (2015) A protocol for variable-resolution first-order reversal curve measurements. Geochemistry, Geophysics, Geosystems, 16, 1364–1377.

The "fate rock" or "magnet mountain" which ruined every ship coming too close by pulling out all nails due to its terrible magnetic power 2.

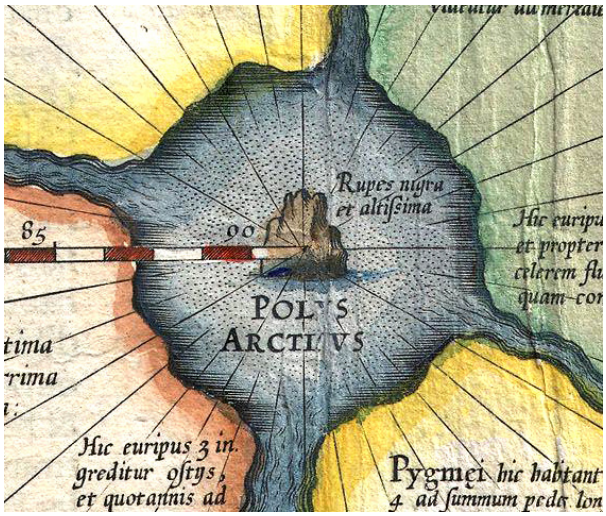

The Rupes Nigra, a phantom island, was believed to be a 33-mile-wide black rock located at the Magnetic North Pole or at the North Pole itself. It purportedly explained why all compasses point to this location.

The IRM Quarterly

The *Institute for Rock Magnetism* is dedicated to providing state-of-the-art facilities and technical expertise free of charge to any interested researcher who applies and is accepted as a Visiting Fellow. Short proposals are accepted semi-annually in spring and fall for work to be done in a 10-day period during the following half year. Shorter, less formal visits are arranged on an individual basis through the Facilities Manager.

The *IRM* staff consists of **Subir Banerjee**, Professor/Founding Director; **Bruce Moskowitz**, Professor/Director; **Joshua Feinberg**, Assistant Professor/Associate Director; **Mike Jackson, Peat Sølheid** and **Dario Bilardello**, Staff Scientists.

Funding for the *IRM* is provided by the **National Science Foundation**, the **W. M. Keck Foundation**, and the **University of Minnesota**.

The *IRM Quarterly* is published four times a year by the staff of the *IRM*. If you or someone you know would like to be on our mailing list, if you have something you would like to contribute (*e.g.*, titles plus abstracts of papers in press), or if you have any suggestions to improve the newsletter, please notify the editor:

Dario Bilardello
Institute for Rock Magnetism
Department of Earth Sciences
University of Minnesota
150 John T Tate Hall
116 Church Street SE
Minneapolis, MN 55455-0128
phone: (612) 624-5274
e-mail: dario@umn.edu
www.irm.umn.edu

UNIVERSITY OF MINNESOTA

The New IRM lab

is featured in a short
University of Minnesota video
for the
Tate Hall Grand Opening
(March 7-8th).

Check it out at:
https://youtu.be/y-RqI1tYWK8